ELSEVIER

Contents lists available at ScienceDirect

# Chemical Geology

journal homepage: www.elsevier.com/locate/chemgeo





# Effects of contact metamorphism on the lithium content and isotopic composition of kerogen in coal

Zebadiah Teichert a,\*, Cortland F. Eble b, Maitrayee Bose A, Lynda B. Williams

- <sup>a</sup> School of Earth and Space Exploration, Arizona State University, Tempe, AZ 85287-1404, United States of America
- b Kentucky Geological Survey, Lexington, KY 40506, United States of America

#### ARTICLE INFO

Editor: Oleg Pokrovsky

Keywords:
Lithium isotopes
Coal
Kerogen
Maceral
Contact metamorphism
Secondary Ion Mass Spectrometry (SIMS)

#### ABSTRACT

Lithium isotopes ( $\delta^7$ Li) in coals have been shown to increase with thermal maturity, suggesting preferential release of  $^6$ Li from kerogen to porefluids. This has important implications for paleoclimate studies based on  $\delta^7$ Li of buried marine carbonates, which may incorporate Li from porefluids during recrystallization. Here, the Li content and isotopic composition of macerals from two coal seams intruded by dikes, were studied as a function of temperature across a thermal gradient into the unmetamorphosed coal. Samples were collected in Colorado (USA) from a Vermejo Fm. coal seam intruded by a mafic-lamprophyre dike and compared to a Dutch Creek No.2 coal seam intruded by felsic-porphyry dike; a potential source of Li-rich fluids.

The Li-content and Li-isotope compositions of coal macerals were measured in situ by Secondary Ion Mass Spectrometry (SIMS). The macerals of the Vermejo coal samples, buried to VR $_0$  0.68% ( $T_{max}=104\,^{\circ}$ C), contained <1.5  $\mu$ g/g Li with an average vitrinite  $\delta^7$ Li of  $-28.4\pm1.6\%$ , while liptinite and inertinite were heavier, averaging  $-15.4\pm3.6\%$  and  $-10.5\pm3.7\%$ , respectively. The contact metamorphosed vitrinite/coke showed the greatest change with temperature with  $\delta^7$ Li 18 to 37% heavier than the unmetamorphosed vitrinite.

The Dutch Creek coal, buried to VRo 1.15% ( $T_{max}=147\,^{\circ}\text{C}$ ), prior to dike emplacement, may have released Li during burial, as less isotopic change was observed between contact metamorphosed and unmetamorphosed macerals. Overall, Li contents were  $<1~\mu\text{g/g}$ , and the vitrinite in metamorphosed coal had  $8^{7}\text{Li}$  values 8 to 21% heavier than the unmetamorphosed coal. SIMS measurements on macerals near the dike did not show an increase in Li-content indicative of Li derived from dike fluids, however previous bulk measurements that included silicates showed slightly higher (2-3  $\mu\text{g/g}$ ) Li-contents near the dike, suggesting possible Li incorporation from dike fluid into metamorphic silicates. A negative correlation was observed between Li-content and  $^{12}\text{C}^+/^{30}\text{Si}^+$  count ratios, indicating that at metamorphic temperatures Li becomes concentrated in silicates.

#### 1. Introduction

Kerogen is the most abundant form of organic matter on earth and kerogen bearing rocks, such as coal, are in some cases potential sources of lithium (Li) (Qin et al., 2015) but have been largely overlooked in studies of Li geochemical cycles (Teichert et al., 2020). Lithium and its stable isotopes (<sup>7</sup>Li and <sup>6</sup>Li) are used to trace many dynamic earth processes because the relatively large mass difference between the isotopes (~17%) results in a terrestrial fractionation of up to ~70% (Penniston-Dorland et al., 2017; Tomascak et al., 2016). Lithium isotopes have been utilized in >50 studies related to continental weathering over the past two decades, in part because the Li-isotope system traces the chemical weathering of silicates which consume atmospheric

CO<sub>2</sub> (Berner et al., 1983; Kump et al., 2000). During primary silicate dissolution there is limited Li-isotope fractionation, however secondary minerals which form during weathering preferentially incorporate <sup>6</sup>Li (Pogge von Strandmann et al., 2020). The ratio of primary silicate dissolution to secondary mineral formation, coined 'the weathering congruency', is controlled by the climate at a given time (Pogge von Strandmann et al., 2020). Lithium from silicate weathering accumulates in the dissolved load of rivers and groundwater with a Li-isotope composition determined by the weathering congruency and accounts for ~50% of the Li input into seawater (Hathorne and James, 2006). Thus, the Li-isotopic composition of seawater at a given time, contains information about global weathering and therefore climate, which is a major driver of continental weathering (Kennedy and Wagner, 2011;

<sup>\*</sup> Corresponding author at: Physical Sciences F-686, 550 E. Tyler Mall, Arizona State University, Tempe, AZ 85287-1404, United States of America. E-mail address: zteicher@asu.edu (Z. Teichert).

Pogge von Strandmann et al., 2020). The Li-isotope composition of seawater can be recorded by inorganic or biogenic carbonates forming in the marine environment and have been used to reconstruct paleoclimate (Lechler et al., 2015; Misra and Froelich, 2012; Pogge von Strandmann et al., 2017; Pogge von Strandmann et al., 2013; Ullmann et al., 2013), which may be valid if there is no overprinting of the carbonate Li-isotope signature during diagenesis (Dellinger et al., 2020).

Kerogen has been identified as a potential source of isotopically light Li and it has been proposed that Li is released from kerogen into porefluids during diagenesis at the temperatures of oil and gas generation and can be useful in tracing hydrocarbons (Williams et al., 2012; 2013; 2015). Accordingly, formation waters tend to have lighter isotope ratios  $(\delta^7 \text{Li} + 4 \text{ to } + 16\%; \text{ Collins}, 1975; \text{ Eccles and Berhane}, 2011; \text{ Mac$ pherson et al., 2014; Millot et al., 2011; Phan et al., 2016) than lakes (+17 to +36%; Chan and Edmond, 1988; Tomascak et al., 2003; Witherow et al., 2010), rivers (mean + 23%; Penniston-Dorland et al., 2017; Tomascak et al., 2016) and seawater ( $\delta^7 \text{Li} \sim +31\%$ ; Chan and Edmond, 1988; You and Chan, 1996). In a survey of coals from basins across the United States, Teichert et al. (2020) found that low-rank coals are isotopically lighter (-10% to -20%) than most thermally mature coals (-5% to +5%) irrespective of age or sedimentary basin (Fig. 1) suggesting that <sup>6</sup>Li is preferentially released from kerogen into porefluids during thermal maturation and hydrocarbon generation. This is consistent with the finding that up to 50% of the Li in low rank coals can be associated with organic matter (OM) whereas Li is almost entirely associated with silicates in high rank coals (bituminous to anthracite) (Dai et al., 2021; Finkelman et al., 2018). Low-rank coals contain 10 μg/g Li on average (Ketris and Yudovich, 2009) and it has been hypothesized that many inorganic elements, such as Li, bond to carboxylic acid (COOH), and phenolic hydroxyl groups (OH) to form chelates during peatification; a precursor to coal formation (Swaine, 1990). With increasing coal rank (thermal maturity) volatiles are lost and OM releases various hydrocarbons. The C - C and C - H bonds in the OM are strengthened causing the weakly bound inorganic heteroatoms to be expelled via demetallation and decarboxylation reactions and aromatization (Filby and van Berkel, 1987; Li et al., 2010).

In this study we examined the effect of thermal maturity on the Licontents and isotopic compositions across two coal seams from Colorado (USA), which have been altered by contact metamorphism. Varying temperatures of contact metamorphism across a single coal seam allows comparison to the unmetamorphosed coal which experienced only burial diagenetic temperatures ( $<150\,^{\circ}$ C). The Li-contents and isotopic changes across the contact metamorphosed coal seams are used as an analog for increasing coal rank while it is recognized that the

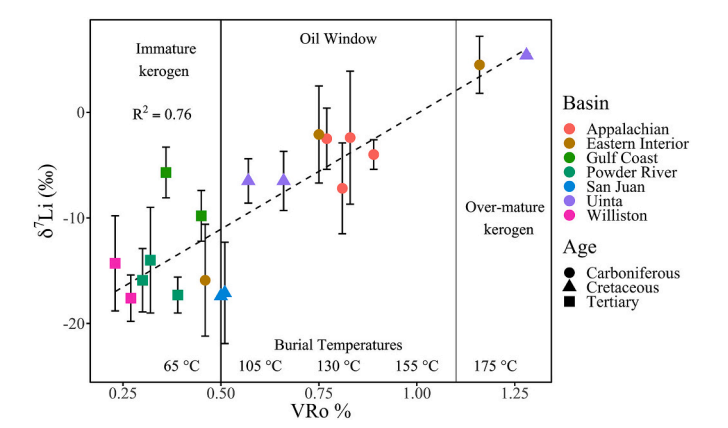


Fig. 1. Scatter plot showing a correlation between vitrinite reflectance (VR<sub>o</sub> ‰) and  $\delta^7 \text{Li}$  measurements of coal samples from different sedimentary basins (color) and of different ages (shape) from across the United States (Teichert et al., 2020). The  $\delta^7 \text{Li}$  values shown here have been corrected by +10‰ based on an analytical matrix effect described in Teichert et al. (2022).

metamorphic heating is rapid compared to burial so that reaction mechanisms will differ. The aim of this study was to evaluate the range of  $\delta^7 \text{Li}$  in coal macerals and their change during thermal alteration. The importance of this work is that Li released from kerogen into sedimentary porefluids can affect the  $\delta^7 \text{Li}$  of other authigenic minerals incorporating organic sources of Li. This should be recognized particularly in studies of buried marine sediments used to interpret paleoclimate.

#### 2. Materials and methods

#### 2.1. Samples and geologic settings

The Morley Dike is a mafic lamprophyre dike which is exposed in outcrop where it cuts across sedimentary rocks of the Upper Cretaceous Vermejo Fm. in the Raton Basin of South-Central Colorado, USA (Cooper et al., 2007; Johnson, 1969) (Fig. 2a). Samples were collected from a high volatile bituminous B coal seam in contact with the dike (Fig. 2b). The Morley Dike has a thickness of 1.6 m, a strike of 114° and is locally vertical where it contacts sedimentary layers which have a local strike of 14° and a dip of 16°. The coal seam, sampled on the north side of the Morley Dike, has an average exposed thickness of 1.1 m and is exposed laterally for approximately 16 m. The coal seam was sampled within a ~ 4 m thick sedimentary unit with alternating layers of coal benches and shaley coal forming talus slopes. The coal rich unit is bounded by sandstone units above and beneath as displayed in the stratigraphic column (Fig. 3). Coal and coke samples were collected from the middle ~0.3 m of the 1.1 m coal seam. Five samples were collected within the contact aureole zone of the coal seam and one coal sample was collected far from the dike (3.26 m) to determine the baseline composition of the coal prior to contact metamorphism. This sample is unmetamorphosed, having experienced temperatures <200 °C, and pressures <300 MPa (Coombs, 1961). At each sampling location, samples were recovered at least 10 cm into the exposed surface to avoid highly weathered samples. Presumably the coal macerals that were contact metamorphosed had a similar composition to the unmetamorphosed coal seam prior to being altered by the intrusion.

Additionally, four samples were obtained from the Dutch Creek No. 2 mine in the Piceance Basin (west-central Colorado), a medium volatile bituminous coal seam adjacent to a 1.5 m thick felsic porphyry dike, which intruded the coal seam at a 60° angle from bedding (Bostick and Collins, 1987). These samples were chosen to evaluate the potential addition of Li from fluids associated with a felsic dike compared to the mafic Morley Dike. These Upper Cretaceous coal samples were collected (and donated for this study) by Bostick and Collins (1987), who determined the coal/coke sample compositions and VRo (% vitrinite reflectance using an oil immersion objective). The Dutch Creek No. 2 mine coal is found in the Bowie Shale Mbr. of the Williams Fork Fm. (Hettinger et al., 2000). The chemical content of 66 elements in this sample suite (including Li) were reported by Finkelman et al. (1998) who found that 45 lithophile elements (including Li) had maximum contents at the heated coal and low volatile coke transition zone (31 cm from the dike (0.21 X/D)) where silicates such as illite and kaolinite were abundant (25 wt% of mineral matter).

#### 2.2. Analytical methods

Vermejo coal samples were prepared according to procedures described by the American Society for Testing and Materials (ASTM) D2013/D2013M-18 (ASTM, 2018a) by first crushing them to -8 mesh (2.36 mm screen openings) using a hammermill crusher. The samples were then halved using a sample riffler with one half being re-bagged for storage. The other half was further reduced in size to -20 mesh (850  $\mu$ m screen openings) using a plate-grinding mill and split again. One split of -20 mesh coal was used for the construction of coal petrographic pellets. The other split was further reduced in size to -60 mesh (250  $\mu$ m screen openings), using a pulverizer, for proximate and total carbon/

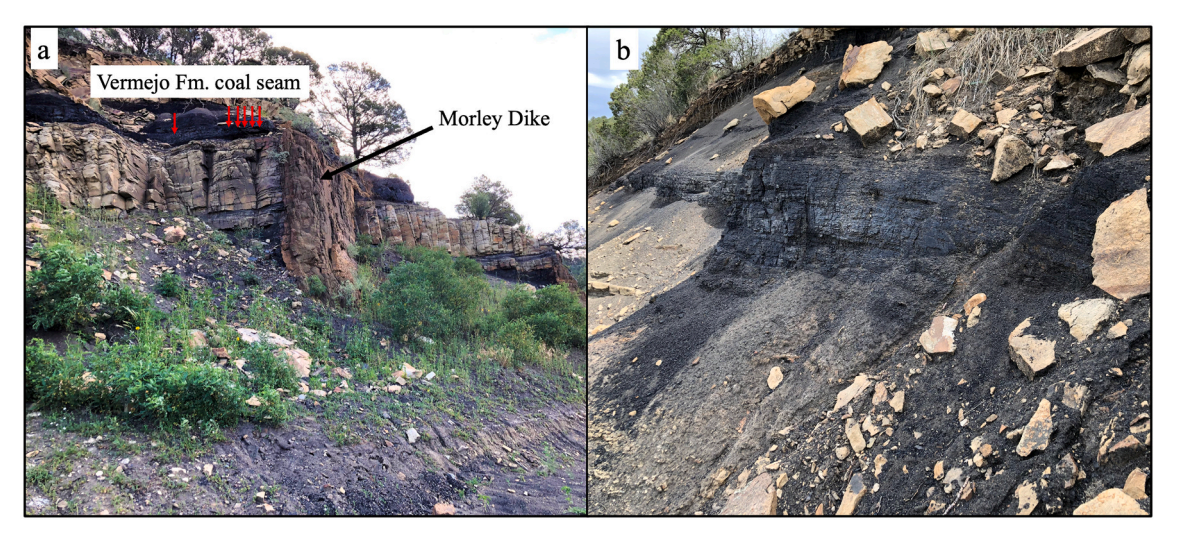


Fig. 2. Photographs of the (a) outcrop and (b) coal seam where contact metamorphosed Vermejo Fm. coals were collected adjacent to the mafic lamprophyre 'Morley' dike.

sulfur analyses. The equipment used was blown out with compressed air and wiped down with disposable towels and isopropyl alcohol between each successive sample.

#### 2.2.1. Geochemistry

Proximate analyses were performed according to ASTM D7582–15 using a Leco TGA 701 analyzer (ASTM, 2015). Total carbon/sulfur analyses were performed according to ASTM D4239-18e1 using a Leco SC-432 carbon/sulfur analyzer (ASTM, 2018b). All values, except for moisture content, are reported on a weight percent, dry basis unless noted otherwise. Mineral matter was calculated from ash and sulfur data using the Parr formula (Parr, 1922, 1928), where:

Mineral Matter (wt%, dry basis) = 
$$(Ash \times 1.08) + (Sulfur \times 0.55)$$
 (1)

# 2.2.2. Petrology

Coal petrographic pellets were constructed from the -20-mesh material by mixing 5 g of coal with epoxy resin in 3.2 cm diameter phenolic ring molds and allowed to cure. Upon hardening, samples were polished with a final grit size 0.04  $\mu m$  with colloidal silica. Samples were point counted using a Zeiss Universal reflecting, and transmitting, light microscope equipped with both white and fluorescent (UV) light sources. Maceral percentages are based on 500-point counts of organic material for each sample, in accordance with ASTM D2799–13 (ASTM, 2013) and are reported on a volume percent, mineral matter free (vol%, mmf) basis. Whole coal maceral percentages were calculated by including the amount of mineral matter in each sample, converted from weight to volume percent based on ASTM D2799–13 (ASTM, 2013), where:

Mineral Matter<sub>vol</sub>% = 
$$[100 \times (MM_{wt\%}/2.8)]/[((100-MM_{wt\%})/1.2) + (MM_{wt\%}/2.8)]$$
 (2)

Vitrinite reflectance analyses were performed according to ASTM D2798-11a (ASTM, 2011) by first calibrating a Hamamatsu 928A photomultiplier with glass standards of known reflectance. The Schott glass standards used for calibration were SF13–714-276 (0.496%), LaSF9–850-322 (1.009%), and LaSF6–961-349 (1.662%). Following this, 50 random reflectance measurements were collected for each sample using an oil immersion objective ( $R_{\rm o\ random}$ ). Maximum reflectance ( $R_{\rm o\ maximum}$ ) values were calculated from the average  $R_{\rm o\ random}$  values using the conversion formula cited in ASTM D2798-11a (ASTM, 2011), where:

calculated 
$$R_{o \text{ maximum}} = (R_{o \text{ random}} \times 1.09) - 0.034$$
 (3)

Mineral identification was performed on Vermejo coal and coke

samples and the Morley Lamprophyre dike rock using a Malvern PAN-alytical Aeris powder X-Ray Diffractometer with Cu k $\alpha$  radiation. Samples were crushed to  $<\!40~\mu m$  using a BICO Ring and Puck mill. The OM in the two coal samples with the lowest rank was digested in 35%  $H_2O_2$  at  $\sim\!85~$  °C for 3–6 days prior to XRD measurements, following Ward, (1974), while the heavily coked samples were measured without organic oxidation. During  $H_2O_2$  digestion carbonates can also be removed by organic acids that form during the OM digestion process (Ward, 1974). Proximate and ultimate analyses, vitrinite reflectance, mineralogy, and inorganic element determinations for Dutch Creek coal samples were determined previously (Bostick and Collins, 1987; Finkelman et al., 1998).

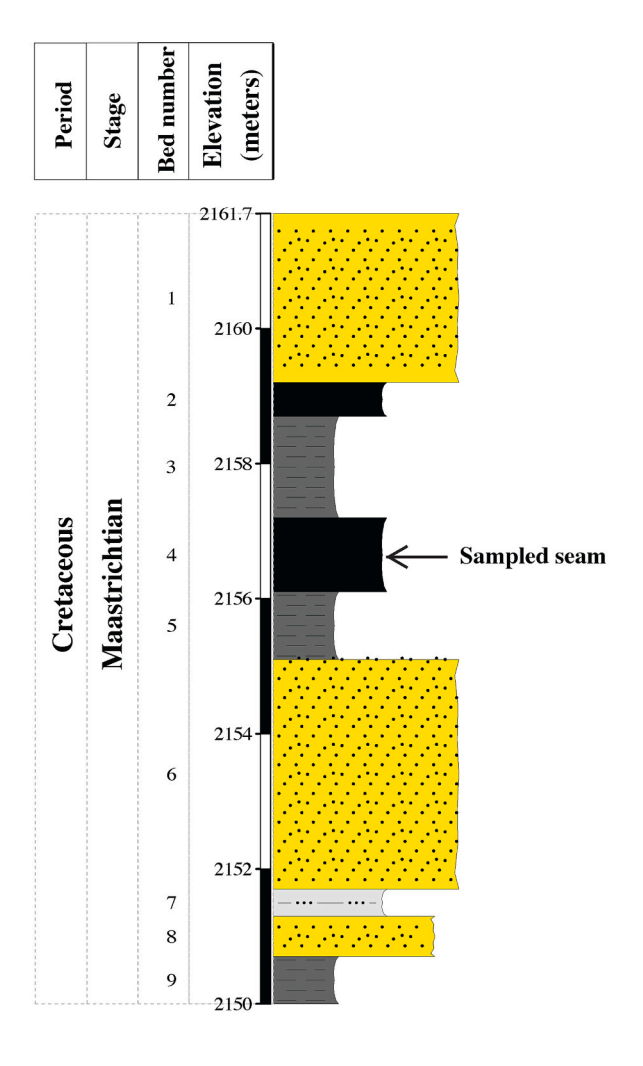
# 2.2.3. Contact metamorphism heat flow and vitrinite reflectance modeling

The maximum temperatures (Tmax) and vitrinite reflectance values reached by coal within the contact aureoles were modeled using the MATLAB® program SILLi 1.0 which was developed by Iyer et al. (2018). This program uses an energy diffusion equation building off of earlier work on the thermal modeling of dikes (Jaeger, 1959, 1957; Lovering, 1935) and calculates the T<sub>max</sub> at each pre-defined time step along a 1-dimensional path adjacent to the intrusion. The input parameters used here are listed in Table S1 along with references. Additionally, the measured mean  $VR_o$  % was used to predict  $T_{\text{max}}$  within the contact aureole using the empirical relationship between experimental pressure bomb temperatures and VR<sub>o</sub> % (Bostick and Pawlewicz, 1984). Burial T<sub>max</sub> values, for the samples outside of the contact aureole, were also determined using measured VR<sub>0</sub> % (Barker and Pawlewicz, 1994). Predicted VR<sub>0</sub> % values were calculated for comparison to measured VR<sub>0</sub> % values using the SILLi 1.0 tool which applies the EASY%Ro method (Sweeney and Burnham, 1990) that uses an Arrhenius reaction model to calculate the maturation of vitrinite with respect to time and temperature.

#### 2.2.4. SIMS analyses

Samples of coal and coke were prepared as <2 mm grains embedded in epoxy and then polished with final grit size of  $<1~\mu m$  colloidal silica. Samples were rinsed in 0.1 M mannitol solution to remove surface adsorbed Li (Teichert et al., 2020) followed by rinsing in de-ionized water that was filtered through AmberSep^TM G26 H (www.dupont. com) to remove trace Li. Conductive gold coats were deposited on the sample surfaces to compensate for sample charging during SIMS analyses.

Li-content and isotopes were measured at Arizona State University in-situ by Secondary Ion Mass Spectrometry (SIMS) using a Cameca



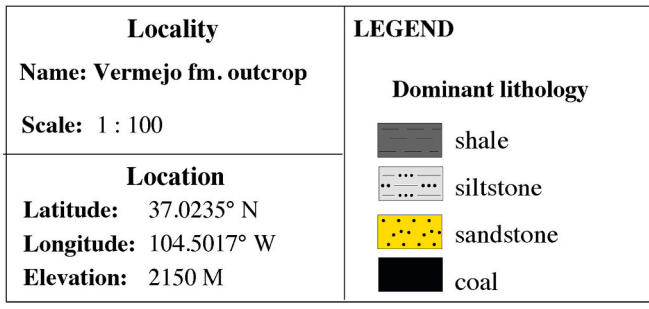


Fig. 3. Stratigraphic column of Vermejo Fm. outcrop adjacent to the Morley Dike.

(Ametek Inc.) IMS-6f instrument to evaluate the Li-content and isotopic composition of different coal components including macerals and coke. Sample maps were made with a reflected light petrographic microscope, and effort was made to measure macerals while avoiding silicate minerals. An  $\rm O_2^-$  primary ion beam was accelerated toward the sample surfaces at  $\rm -12.6~keV$  and defocused to a  $\rm \sim 30$  to 50  $\mu m$  diameter spot on the sample which was held at  $\rm +5~kV$  for a total impact energy of  $\rm +8.8~keV$  per primary atom impact. Impacting primary ions sputter off secondary atoms, electrons and ions from the sample surface (Sigmund, 1969). Positive secondary ions were detected using an electron multiplier detector after being separated by energy and mass/charge, using an electron multiplier detector. Mass interferences were eliminated by adjusting the entrance and exit slits to the mass spectrometer to increase the mass resolving power (MRP = mass/ $\rm \Delta mass$ ) to  $\rm \sim 1000$ . This MRP

was sufficient to resolve isobaric mass interferences which were  $^{24}\text{Mg}^{2+}$  and  $^{11}\text{BH}^+$  interfering with  $^{12}\text{C}^+$ ,  $^{14}\text{N}^{2+}$  interfering with  $^{7}\text{Li}^+$  and  $^{12}\text{C}^{2+}$  interfering with  $^{6}\text{Li}^+$ .

For Li-content measurements, high energy  $^7\text{Li}^+$ ,  $^{12}\text{C}^+$  and  $^{30}\text{Si}^+$  ions were monitored using a sample voltage offset of -75 V to count only high energy ions thus removing molecular interferences (Hervig et al., 2006) and to reduce counts enough for all species to be measured on the electron multiplier detector. Using all the settings described above has been shown to simplify the determination of Li-contents, based on measured  $^7\text{Li}^+/^{12}\text{C}^+$  ratios, by eliminating matrix effects caused by variations sample O-contents (Teichert et al., 2022). The measured  $^7\text{Li}^+/^{12}\text{C}^+$  ratios of each spot measurement were used to determine the Li-contents using the Li-ion implanted polycarbonate standard described in Teichert et al. (2022), which has H-C-O abundances similar to kerogen. The homogenous polycarbonate Li-implant standard was measured prior to analyses of coal samples to determine the Li-content calibration factor (k\* =142) used to determine Li content with the following expression.

Li ppm atomic = 
$$(^{7}\text{Li}^{+}/^{12}\text{C}^{+} \times \text{k}^{*}) \times C_{af} \times 1.0832$$
 (4)

where:

 $C_{af}$  = Carbon atom fraction of the sample being measured.

 $1.0832 = (^{6}\text{Li} + ^{7}\text{Li})/(^{7}\text{Li})$  to account for  $^{6}\text{Li}$ 

After determining the Li ppm atomic, contents were converted to wt. ppm ( $\mu g/g$ ) using the stoichiometry of each sample.

Note that the Li-content standard (polycarbonate) lacks any significant contribution of inorganic elements commonly present in kerogen that might alter the secondary ion yields of both <sup>7</sup>Li<sup>+</sup> and <sup>12</sup>C<sup>+</sup>. For SIMS spot analyses where inorganic elements have concentrations >1% trace element calibrations become more approximate (Williams, 1985).

Lithium isotope ratios are reported as the per mille deviation from the LSVEC standard (Flesch et al., 1973) with the following expression.

$$\delta^7 \text{Li\%o} = \left(\frac{R_{Sample} - R_{Standard}}{R_{Standard}}\right) \times 1000 \tag{5}$$

where  $R = {}^{7}\text{Li}/{}^{6}\text{Li}$  and the standard is NIST SRM 612 (R = 12.0192).

For isotope measurements,  $^7\text{Li}^+$  and  $^6\text{Li}^+$  were both monitored with no energy offset. To determine the instrumental mass fractionation (IMF), measurements of the NIST SRM 612 silica-based glass with a certified Li content of 40 µg/g (SRM 612 certificate, 2012) and  $\delta^7\text{Li}$  values of +32% (Bluztajn et al., 2004) were taken before and after measurements of unknown samples. NIST SRM 612 standard measurements produced consistent values of the IMF ( $2\sigma_x \pm 1.4\%$ ) during each analytical session. Isotope ratios measured on coal macerals were corrected by +10% because of a matrix effect between the NIST SRM 612 glass and organic materials (Teichert et al., 2022).

#### 3. Results

The sample distances from the igneous dikes, proximate analysis and average random vitrinite reflectance (VRo %) values are summarized in Table 1. For the Vermejo and Dutch Creek coals the volatile matter decreased while the ash yield, mineral matter and the average VRo % increased with increasing proximity to the dike. Table 2 shows the wt% of coke and major maceral groups of the coals studied (detailed organic petrology shown in Supplementary Information, Table S2), the minerals present in each sample (in order of abundance) and the mineral matter vol%. Notably, the coke content of the coal increases closer to the dike as the volatile matter is lost from vitrinite and liptinite macerals. Representative reflected light microscope images showing analytical craters in different macerals and coke in select Vermejo and Dutch Creek coals are shown in Figs. 4 and 5. The macerals type/coke,  $\delta^7$ Li values, Li-contents and <sup>12</sup>C<sup>+</sup>/<sup>30</sup>Si<sup>+</sup> ratios for spot analyses are tabulated below each figure (Tables 3 and 4). All individual spot analyses measured in this study can be found in Table S3. Crater sizes vary based on the primary beam

**Table 1**Some values from Proximate analyses of Coal and Coke samples.

| Sample    | Distance from<br>Dike (cm) | Residual Moisture<br>(wt%, ar) | Volatile Matter (wt<br>%, dry) | Ash yield (wt<br>%, dry) | Mineral Matter (wt<br>%, dry) | Total carbon (wt<br>%, dry) | Total sulfur (wt<br>%, dry) | Avg. VR <sub>o</sub><br>random (%) |
|-----------|----------------------------|--------------------------------|--------------------------------|--------------------------|-------------------------------|-----------------------------|-----------------------------|------------------------------------|
| Vermejo S | Samples                    |                                |                                |                          |                               |                             |                             |                                    |
| V-A       | 4                          | 1.0                            | 6.0                            | 35.8                     | 38.8                          | 60.9                        | 0.20                        | 4.09                               |
| V-B       | 34                         | 1.9                            | 9.3                            | 25.4                     | 27.7                          | 68.4                        | 0.45                        | 3.92                               |
| V-C       | 84                         | 2.1                            | 10.5                           | 19.8                     | 21.7                          | 72.9                        | 0.55                        | 3.14                               |
| V-D       | 123                        | 2.1                            | 11.3                           | 16.2                     | 17.9                          | 76.6                        | 0.59                        | 3.03                               |
| V-E       | 143                        | 4.0                            | 29.8                           | 12.3                     | 13.6                          | 70.9                        | 0.62                        | 1.02                               |
| V-UM      | 330                        | 5.6                            | 37.9                           | 5.7                      | 6.5                           | 73.7                        | 0.64                        | 0.68                               |
| Dutch Cre | eek Samples (Bostick       | and Collins, 1987;Finkelr      | nan et al., 1998 <b>)</b>      |                          |                               |                             |                             |                                    |
| DC-B      | 9                          | 1.3                            | 13.0                           | 19.1                     | 20.9                          | 70.9                        | 0.54                        | 4.86                               |
| DC-D      | 24                         | 1.4                            | 10.6                           | 9.2                      | 10.4                          | 83.0                        | 0.89                        | 3.91                               |
| DC-F      | 42                         | 0.7                            | 13.6                           | 7.2                      | 8.1                           | 83.1                        | 0.58                        | 2.03                               |
| DC-K      | 106                        | 0.7                            | 28.0                           | 4.8                      | 5.4                           | 83.7                        | 0.45                        | 1.15                               |

VRo- vitrinite reflectance in oil; ar stands for "as recieved". The Dutch Creek samples use the same naming scheme used in Finkelman et al. (1998).

**Table 2**Major maceral groups and minerals present in coal and coke samples.

| Sample         | Distance from Dike (cm)   | Vitrinite (wt%, dmmf) | Inertinite (wt%, dmmf) | Liptinite (wt%, dmmf) | Coke (wt%, dmmf) | Minerals present                       | Mineral Matter (vo<br>%, dry) |
|----------------|---------------------------|-----------------------|------------------------|-----------------------|------------------|--|-------------------------------|
| Vermejo Sa     | mples                     |                       |                        |                       |                  |  |                               |
| V-A            | 4                         | 0.0                   | 24.8                   | 0.0                   | 75.2             | qtz                                    | 23.4                          |
| V-B            | 34                        | 0.0                   | 23.2                   | 0.0                   | 76.8             | qtz, kao                               | 15.6                          |
| V-C            | 84                        | 0.0                   | 23.2                   | 0.0                   | 76.8             | qtz, kao                               | 11.8                          |
| V-D            | 123                       | 0.0                   | 17.6                   | 0.0                   | 82.4             | qtz, kao                               | 9.5                           |
| V-E            | 143                       | 48.0                  | 13.2                   | 1.6                   | 37.2             | qtz, dck, vrm, aer kao                 | 7.1                           |
| V-UM           | 330                       | 67.2                  | 29.2                   | 3.6                   | 0.0              | qtz, kao, dck, vrm, ame, aer           | 3.2                           |
| Morley<br>Dike | NA                        | NA                    | NA                     | NA                    | NA               | bar, crn, chl, dck, kao, bt, cal, aug  | NA                            |
|                | k Samples (Bostick and Co |                       |                        |                       |                  |  |                               |
| DC-B           | 9                         | nm                    | nm                     | nm                    | nm               | cal, ank, qtz, fs, sd, py, hm          | *10.5                         |
| DC-D           | 24                        | nm                    | nm                     | nm                    | nm               | ank, qtz, cal, py, hm, sd, fs          | *5.2                          |
| DC-F           | 42                        | nm                    | nm                     | nm                    | nm               | qtz, ank, kao, sd, ill, py, cal,<br>fs | *4.0                          |
| DC-K           | 106                       | nm                    | nm                     | nm                    | nm               | ank, kao, sd, fs, ill, py, hm,<br>qtz  | *2.7                          |

<sup>\*</sup> Mineral matter vol% approximated from mineral matter wt% for some samples by dividing by 2 following Matjie et al. (2016). dmmf indicates "dry mineral matter free"; nm = not measured; NA = not applicable. Qtz = Quartz; Kao = Kaolinite; Dck = Dickite; Vrm = Vermiculite; Aer = Aerinite; Ame = Amesite; Bar = Barite; Crn = Corundum; Chl = Chlorite; Bt = Biotite; Cal = Calcite; Aug = Augite; Ank = Ankerite; Sd = Siderite; Ill = Illite; Fsp = Feldspar group; Py = Pyrite; Hm = Hematite.

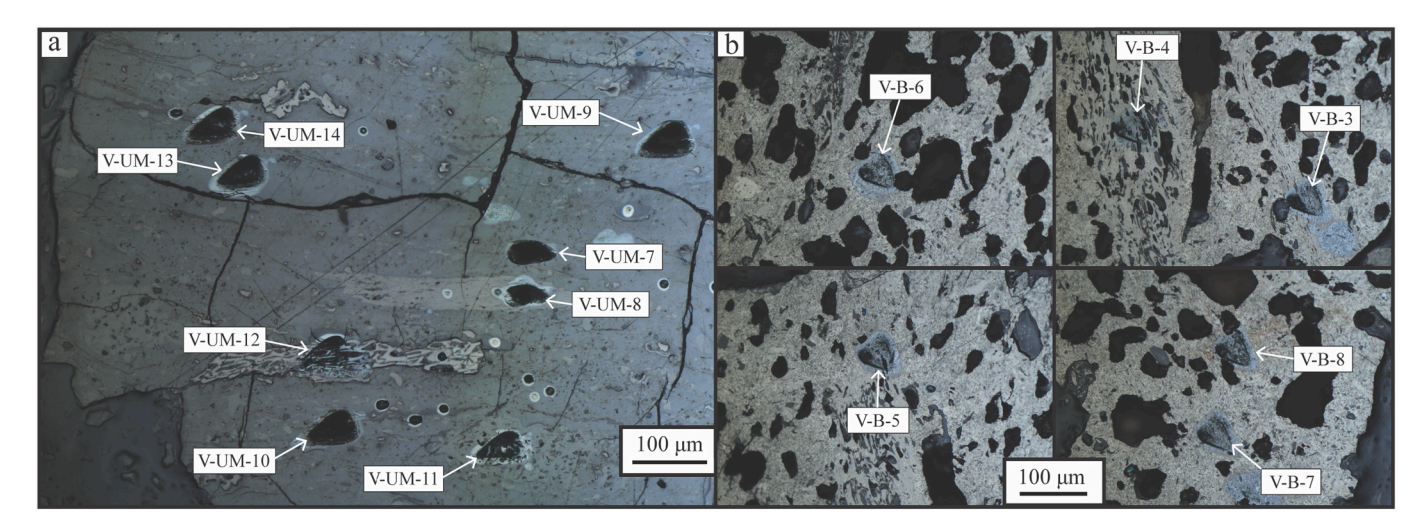


Fig. 4. Reflected light microscope images of Vermejo coal samples (a) V-UM and (b) V-B with analytical craters labeled.

current used. For macerals with very low Li-contents it was necessary to use higher primary beam currents to obtain enough counts for statistically significant Li-isotope ratios. Table 5 summarizes Li-contents

determined by bulk techniques (Finkelman et al., 1998) as well as mean Li-contents and  $\delta^7 \text{Li}$  values of multiple spot analyses made on different organic maceral types in this SIMS study. The large  $2\sigma$  values

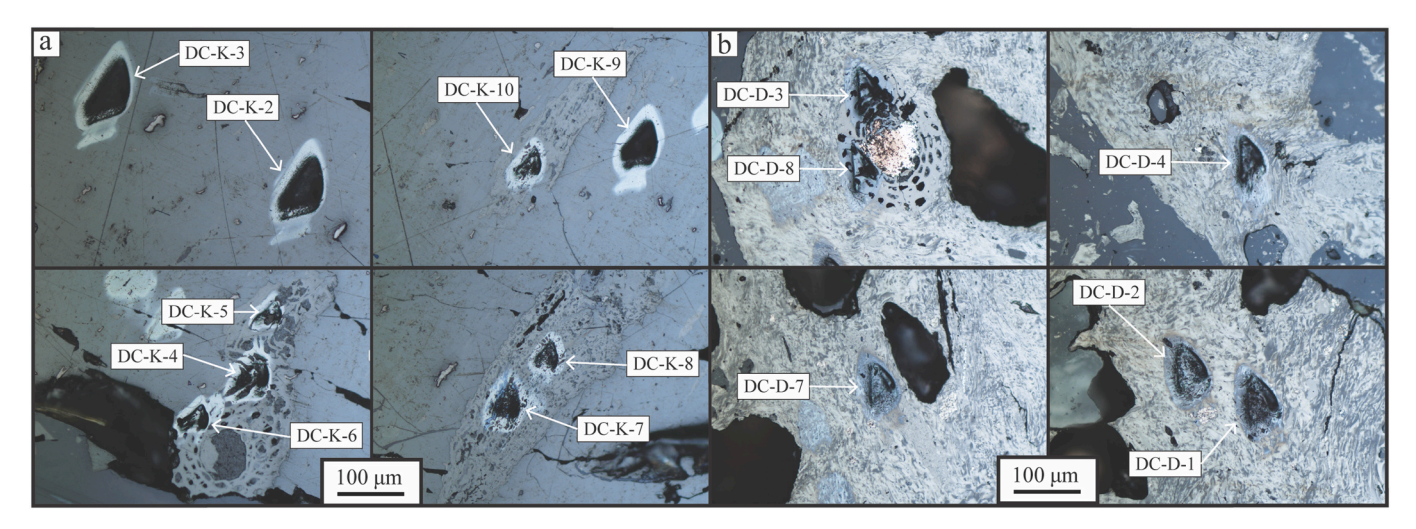


Fig. 5. Reflected light microscope images of Dutch Creek coal samples (a) DC-K and (b) DC-D with analytical craters labeled. Analytical craters vary in size according to the primary current used.

**Table 3**SIMS results for selected Vermejo coal spot measurements.

| Measurement | Primary<br>maceral or<br>coke | δ <sup>7</sup> Li<br>(‰) | S.E.<br>(‰) | P.E.<br>(‰) | Li<br>(μg/<br>g) | <sup>12</sup> C <sup>+</sup> / <sup>30</sup> Si <sup>+</sup> |
|-------------|-------------------------------|--------------------------|-------------|-------------|------------------|--|
| V-UM-7      | Vitrinite                     | -37.8                    | 1.9         | 2.2         | 0.23             | 9.37   |
| V-UM-8      | Inertinite                    | -22.9                    | 2.2         | 2           | 0.14             | 147.70   |
| V-UM-9      | Vitrinite                     | -30.0                    | 1.9         | 2.1         | 0.20             | 31.97  |
| V-UM-10     | Vitrinite                     | -21.0                    | 2.3         | 2.4         | 0.21             | 23.55  |
| V-UM-11     | Inertinite                    | -14.0                    | 1.1         | 1           | 0.78             | 1.42   |
| V-UM-12     | Inertinite                    | -7.1                     | 0.7         | 0.8         | 1.67             | 0.92   |
| V-UM-13     | Vitrinite                     | -26.8                    | 1.9         | 2.1         | 0.33             | 7.26   |
| V-UM-14     | Liptinite                     | -19.2                    | 2           | 2.4         | 0.26             | 16.90  |
| V-B-3       | Coke                          | 2.8                      | 1.4         | 1.3         | 0.37             | 4.22   |
| V-B-4       | Inertinite                    | -0.3                     | 1.2         | 1           | 0.41             | 12.73  |
| V-B-5       | Coke                          | 9.0                      | 0.9         | 0.9         | 0.55             | 2.96   |
| V-B-6       | Coke                          | 11.8                     | 1           | 1           | 0.82             | 2.02   |
| V-B-7       | Coke                          | 10.3                     | 0.9         | 1           | 0.46             | 2.16   |
| V-B-8       | Coke                          | 7.3                      | 0.7         | 0.8         | 1.05             | 1.40   |

Standard error (S.E.) and Poisson error (P.E.) are  $1\sigma.$  V-UM is the distal coal sample and V-B is 34 cm from the dike.

 Table 4

 SIMS results for selected Dutch Creek coal spot measurements.

| Measurement | Primary<br>maceral or<br>coke | δ <sup>7</sup> Li<br>(‰) | S.E.<br>(‰) | P.E.<br>(‰) | Li<br>(μg/g) | $^{12}\text{C}^{+}/^{30}\text{Si}^{+}$ |  |  |  |
|-------------|-------------------------------|--------------------------|-------------|-------------|--------------|--|--|--|--|
| DC-K-2      | Vitrinite                     | -1.5                     | 1.6         | 1.6         | 0.04         | 831.03                                 |  |  |  |
| DC-K-3      | Vitrinite                     | -0.4                     | 1.5         | 1.3         | 0.31         | 115.03                                 |  |  |  |
| DC-K-4      | Inertinite                    | 9.5                      | 0.4         | 0.5         | 9.82         | 1.35                                   |  |  |  |
| DC-K-5      | Inertinite                    | 4.0                      | 0.5         | 0.5         | 12.46        | 1.17                                   |  |  |  |
| DC-K-6      | Inertinite                    | -4.8                     | 1           | 1.1         | 1.39         | 10.00                                  |  |  |  |
| DC-K-7      | Inertinite                    | 1.8                      | 0.5         | 0.4         | 7.22         | 2.62                                   |  |  |  |
| DC-K-8      | Inertinite                    | 3.7                      | 0.4         | 0.4         | 6.86         | 3.04                                   |  |  |  |
| DC-K-9      | Vitrinite                     | -6.8                     | 1.6         | 1.3         | 0.04         | 727.96                                 |  |  |  |
| DC-K-10     | Inertinite                    | 5.8                      | 0.6         | 0.4         | 5.74         | 3.96                                   |  |  |  |
| DC-D-1      | Coke                          | 8.8                      | 1.1         | 1.1         | 0.34         | 45.87                                  |  |  |  |
| DC-D-2      | Coke                          | 11.8                     | 1           | 1           | 0.46         | 27.58                                  |  |  |  |
| DC-D-3      | Inertinite                    | -3.8                     | 1           | 0.6         | 0.63         | 1.54                                   |  |  |  |
| DC-D-4      | Coke                          | 12.5                     | 0.7         | 0.6         | 0.63         | 33.04                                  |  |  |  |
| DC-D-7      | Vitrinite                     | 4.9                      | 0.8         | 0.9         | 0.76         | 19.22                                  |  |  |  |
| DC-D-8      | Inertinite                    | 2.1                      | 1.3         | 1.3         | 0.25         | 4.18                                   |  |  |  |
|             |                               |                          |             |             |              |  |  |  |  |

DC-K is the country rock sample and DC-D is 24 cm from the dike.

**Table 5**Average Li contents and isotope ratios of coal macerals and coke samples.

| Sample     | Distance<br>from Dike<br>(cm) | Bulk Li<br>contents<br>(μg/g) | Avg. Li<br>contents<br>from SIMS<br>(μg/g) | S.E. | δ <sup>7</sup> Li<br>(‰) | S.E.<br>(‰) | n  |
|------------|-------------------------------|-------------------------------|--|------|--------------------------|-------------|----|
| Vermejo S  | amples                        |                               |  |      |                          |             |    |
| V-A        | 4                             | nm                            |  |      |                          |             |    |
| Coke       |                               |                               | 0.9  | 0.2  | -5.0                     | 4.0         | 5  |
| V-B        | 34                            | nm                            |  |      |                          |             |    |
| Coke       |                               |                               | 0.6  | 0.1  | 9.4                      | 1.4         | 7  |
| Inertinite |                               |                               | 0.4  | NA   | -0.3                     | NA          | 1  |
| V-C        | 84                            | nm                            |  |      |                          |             |    |
| Coke       |                               |                               | 0.7  | 0.04 | 3.0                      | 0.8         | 4  |
| Inertinite |                               |                               | 0.5  | NA   | -3.0                     | NA          | 1  |
| V-D        | 123                           | nm                            |  |      |                          |             |    |
| Coke       |                               |                               | 0.6  | 0.1  | 4.8                      | 1.5         | 3  |
| Inertinite |                               |                               | 1.5  | 1.1  | 11.6                     | 6.1         | 2  |
| V-E        | 143                           | nm                            |  |      |                          |             |    |
| Vitrinite  |                               |                               | 0.9  | 0.3  | -9.5                     | 2.2         | 5  |
| Coke       |                               |                               | 0.8  | 0.2  | -10.8                    | 1.5         | 2  |
| Liptinite  |                               |                               | 0.9  | NA   | -8.3                     | NA          | 1  |
| V-UM       | 330                           | nm                            |  |      |                          |             |    |
| Vitrinite  |                               |                               | 0.3  | 0.04 | -28.4                    | 1.6         | 11 |
| Inertinite |                               |                               | 0.7  | 0.3  | -10.5                    | 3.6         | 5  |
| Liptinite  |                               |                               | 0.2  | 0.1  | -15.4                    | 3.7         | 2  |
| Dutch Cre  | ek Samples                    |                               |  |      |                          |             |    |
| DC-B       | 9                             | 7.1                           |  |      |                          |             |    |
| Coke       |                               |                               | 0.5  | 0.1  | 7.1                      | 2.5         | 4  |
| Inertinite |                               |                               | 0.1  | NA   | -1.4                     | NA          | 1  |
| Vitrinite  |                               |                               | 0.1  | NA   | 14.0                     | NA          | 1  |
| DC-D       | 24                            | 7.1                           |  |      |                          |             |    |
| Coke       |                               |                               | 0.4  | 0.1  | 12.8                     | 1.5         | 5  |
| Inertinite |                               |                               | 0.4  | 0.2  | -0.8                     | 2.9         | 2  |
| Vitrinite  |                               |                               | 0.8  | NA   | 4.9                      | NA          | 1  |
| DC-F       | 42                            | 8.1                           |  |      |                          |             |    |
| Coke       |                               |                               | 0.2  | 0.03 | 9.0                      | 0.8         | 3  |
| Inertinite |                               |                               | 2.3  | 0.5  | -0.9                     | 3.2         | 2  |
| Vitrinite  |                               |                               | 0.3  | NA   | 17.6                     | NA          | 1  |
| DC-K       | 106                           | 4.8                           |  |      |                          |             |    |
| Vitrinite  |                               |                               | 0.1  | 0.1  | -3.3                     | 0.1         | 4  |
| Inertinite |                               |                               | 7.2  | 0.1  | 3.3                      | 0.1         | 6  |

S.E. values are  $2\sigma_{x}.$  Bulk Li contents from Finkelman et al. (1998) for Dutch Creek samples.

 $nm=not\ measured.$ 

(Table 5) show the Li heterogeneity of the samples among the various coal components.

#### 3.1. Heat-flow modeling of contact aureoles

T<sub>max</sub> and VR<sub>0</sub> % values for each sample were plotted against distance from the dike (X) divided by the width of the dike (D) for the Vermejo and Dutch Creek coal samples (Fig. 6). It has been observed that contact aureoles are typically one dike thickness (X/D = 1; Bostick, 1973) or two dike thicknesses (X/D = 2; Dow,1977), thus plotting the distance from the dike as X/D or a percentage of the dike thickness makes it simple to compare contact aureoles of different dike widths (Barker et al., 1998). T<sub>max</sub> values predicted from heat-flow modeling (Iyer et al., 2018) are compared to T<sub>max</sub> values derived from a logarithmic relationship between VR<sub>o</sub> % and T<sub>max</sub> (Bostick and Pawlewicz, 1984), and show a better fit for Dutch Creek coal (Fig. 6c) than for Vermejo Coal sample (Fig. 6a). The burial T<sub>max</sub> values for samples farthest from the igneous dikes (V-UM = 104  $^{\circ}$ C; D-K = 147  $^{\circ}$ C) are indicated by triangles and are significantly lower than T<sub>max</sub> values derived from heat-flow modeling for both contact aureoles. Additionally, measured values for VR<sub>0</sub> % are compared to the EASY%Ro modeled VR<sub>o</sub> % values (Figs. 6b & 7d). As with T<sub>max</sub>, Dutch Creek coal VR<sub>0</sub> % values (Fig. 6d) match SILLi 1.0 modeling results better than the higher temperature Vermejo coal samples (Fig. 6b). Using VR<sub>0</sub> % to determine the width of the contact aureoles, it is observed that the contact aureole is ~1.5 dike widths for the Vermejo coal seam and only ~0.5 dike widths for the Dutch Creek coal seam.

# 3.2. SIMS measurements of Li-contents and Li-isotopes for dike cut coal samples

Finkelman et al. (1998) noted that: 1) removal of elements through volatilization, 2) concentration of refractory phase elements and 3) the loss or addition of elements from fluids (magmatic or hydrothermal) are the three mechanisms by which an igneous intrusion could change the chemical composition of a coal. Although many trace elements remain in refractory phases (e.g., quartz, meta-kaolin), up to 50% of the coal mass

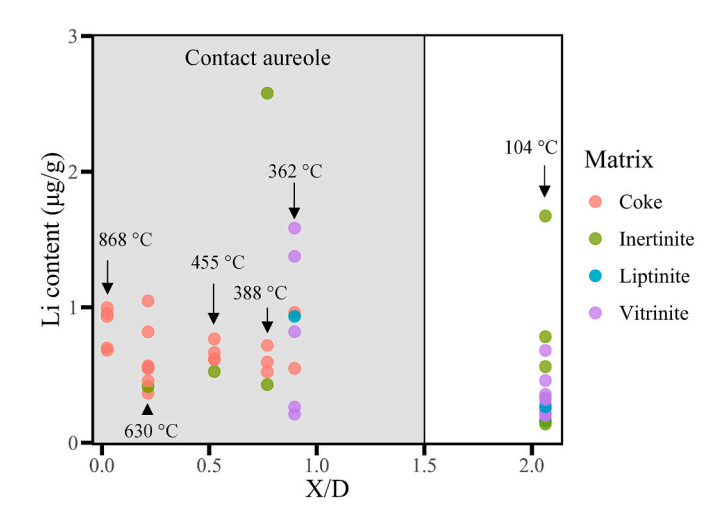


**Fig. 7.** Plot of Li-content measurements corrected for mass loss against X/D for Vermejo coal samples. Points colors indicate maceral type or coke. The contact aureole is shown in gray.  $T_{max}$  values from SILLi 1.0 heat flow modeling are labeled for each sample in the contact aureole. The burial  $T_{max}$  is shown for the UM coal sample outside of the contact aureole. There is significant overlap among the Li-contents of spot measurements from each sample with no clear trend of increasing or decreasing Li-content.

can be lost through the release volatile matter and moisture from organics during the thermal maturation. Therefore, an increase in concentration of a given trace element does not necessarily equate to an addition of that element but mayresult from a loss of mass and residual concentration. Understanding the loss of mass is complicated in contact metamorphic settings where there is likely the addition of mass to the country rock from dike-related fluids precipitating authigenic minerals as chemically active fluids migrate away from the dike.

For the Vermejo coal samples the loss of mass was estimated at  ${\sim}30\%$  in the heavily coked zone (Sample V-A through V-D) and a 10%

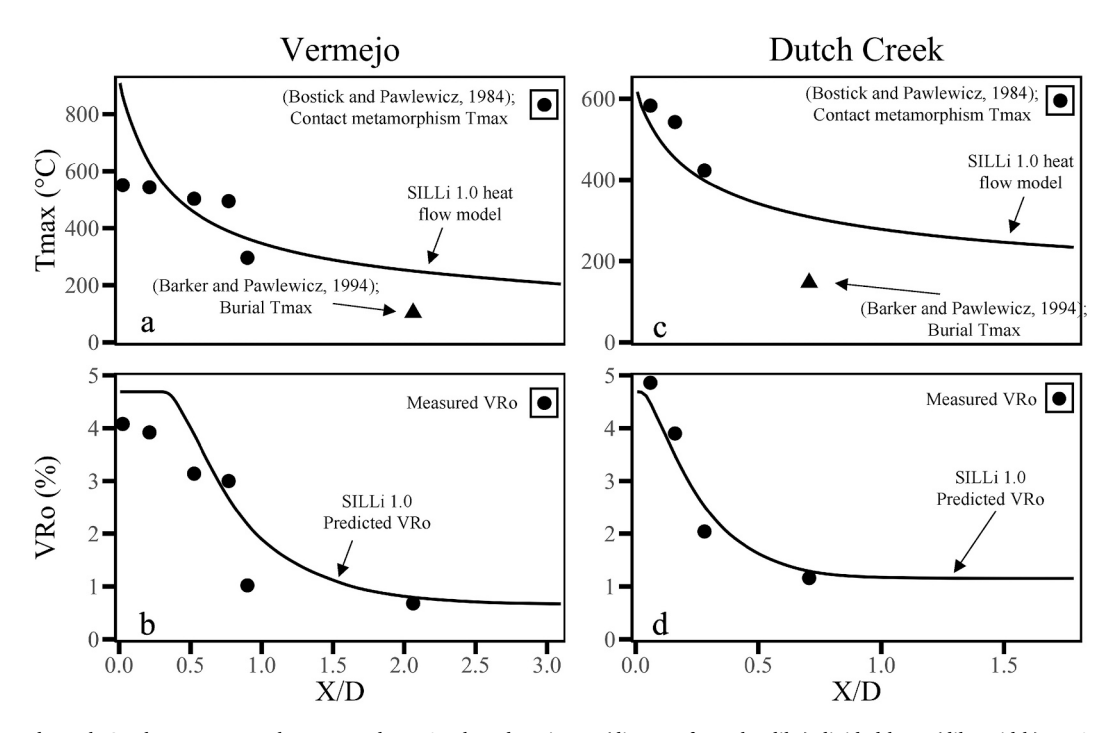


Fig. 6. Vermejo and Dutch Creek contact aureoles  $T_{max}$  and  $VR_o$  % plotted against X (distance from the dike) divided by D (dike width). In 6a and 6c, heat flow modeling  $T_{max}$  values (lines) are compared to  $T_{max}$  values derived from an empirical relationship between  $T_{max}$  and  $VR_o$  (points). Measured  $VR_o$  values (points) are compared to predicted  $VR_o$  values from the EASY%Ro method (lines) in 6b and 6d. The modeled and empirically derived  $T_{max}$  values as well as measured and modeled  $VR_o$  values coincide more closely for the Dutch Creek contact aureole than for the Vermejo contact aureole.

for sample V-E based on changes in volatile matter (Table 1). This mass change was used to correct for elemental compositions of macerals and coke within the contact aureole for comparison to macerals in the unmetamorphosed coal. Finkelman et al. (1998) estimated a total mass loss of 20% for Dutch Creek coal samples within the coked zone and this same estimation was used to correct for Li-contents measured here. Mass loss corrected Li-contents are shown for the Vermejo (Fig. 7) and Dutch Creek (Fig. 8) macerals plotted against X/D.

The Li-contents of the Vermejo macerals and coke overlap among all samples, with mean Li-contents  $\leq \! 1.5~\mu g/g$  and no clear trends. For the Dutch Creek coal, several high Li (5–13  $\mu g/g$ ) inertinite grains were measured on the unmetamorphosed coal samples while the measured vitrinite spots were  $< 0.5~\mu g/g$  for the same sample (Fig. 8). Aside from some high Li inertinite spot analyses in samples DC-K and DC-F the Licontents of all other macerals are  $<1~\mu g/g$  (Fig. 8) with no clear trends related to changes in Li-contents among samples.

The  $\delta^7$ Li values of each measurement are plotted against X/D for the Vermejo coal seam (Fig. 9) and the Dutch Creek coal seam (Fig. 10). Analytical errors of individual measurements are not shown but the mean  $2\sigma_x$  value for a given Li-isotope measurement was  $\pm 2.4\%$ . Large variability in  $\delta^7$ Li was observed, with samples having ranges >8% among different organic maceral types and minerals. Vitrinite macerals were particularly light in the unmetamorhposed coal (-28% for Vermejo coal and - 3% for Dutch Creek coal) compared to the average inertinite and liptinite in those samples (Figs. 9 & 10). The mean  $\delta^7$ Li of the Vermejo unmetamorphosed coal vitrinite was 18 to 37% lighter than vitrinite macerals and coke measured within the contact aureole. Likewise, the  $\delta'$ Li of the Dutch Creek unmetamorphosed coal vitrinite was 8 to 21% lighter than coke and vitrinite within the contact aureole (Table 5). For the Dutch Creek coal samples, the inertinite macerals are isotopically lighter (by 6 to 19‰) than coke and vitrinite within the contact aureole (Fig. 10), but in the unmetamorphosed coal the average inertinite samples are 7% heavier than the average vitrinite.

The Li-contents and  $\delta^7 \text{Li}$  of spot measurements are plotted against the  $^{12}\text{C}^+/^{30}\text{Si}^+$  count ratio for the Vermejo and Dutch Creek coal samples (Figs. 11 & 12). The  $^{12}\text{C}^+$  counts per second (cps) from spot to spot vary up to a factor of 10 although the mean  $2\sigma_x$  in the  $^{12}\text{C}^+$  cps among all carbonaceous spots is only  $\pm 8\%$ . The  $^{30}\text{Si}^+$  cps, however, commonly range over 4 orders of magnitude from spot to spot, thus the change in the  $^{12}\text{C}^+/^{30}\text{Si}^+$  is typically more indicative of changes in the  $^{30}\text{Si}^+\text{cps}$  than  $^{12}\text{C}^+$  cps (Fig. S1). For the Vermejo coal samples there is a weak negative correlation between both the Li-contents (R<sup>2</sup> = 0.48; Fig. 11a)

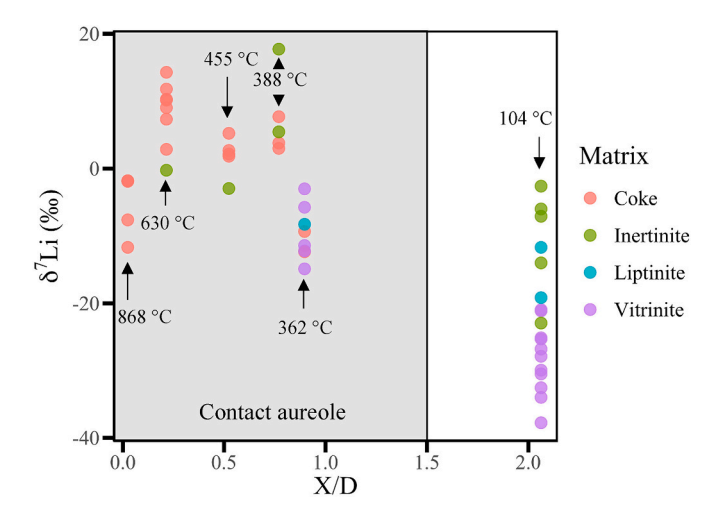


Fig. 9. Plot of  $\delta^7 Li$  measurements against X/D for Vermejo coal samples. The unmetamorphosed coal sample (V-UM) has significantly lower  $\delta^7 Li$  values than samples within the contact aureole with particularly lower  $\delta^7 Li$  among vitrinite macerals.

and  $\delta^7 \text{Li}~(R^2=0.55; \text{Fig. }11b)$  with the  $^{12}\text{C}^+/^{30}\text{Si}^+$  count ratios. For the Dutch Creek coal there is a stronger negative correlation between Licontents and  $^{12}\text{C}^+/^{30}\text{Si}^+$  (R² = 0.74; Fig. 12a) but no correlation between  $\delta^7 \text{Li}$  and  $^{12}\text{C}^+/^{30}\text{Si}^+$  (Fig. 12b). The  $^{12}\text{C}^+/^{30}\text{Si}^+$  ratios on vitrinite macerals in both the mafic and felsic intrusive contact aureoles are higher than the liptinite and inertinite macerals, and coke.

#### 4. Discussion

#### 4.1. Contact aureole temperature modeling

The width of a contact aureole is directly related to several physical properties of the country rock and the intrusion (e.g., thermal diffusivity, temperature, and intrusion width) (Annen, 2017). In addition to the compositional differences between lamprophyre dike intruding the Vermejo coals and the felsic porphyry dike intruding the Dutch Creek coal samples, the major difference was the emplacement temperature. Mafic intrusions are commonly in the temperature range of 900 °C to 1200 °C (Galushkin, 1997; Newcombe et al., 2020; Wang and Manga,

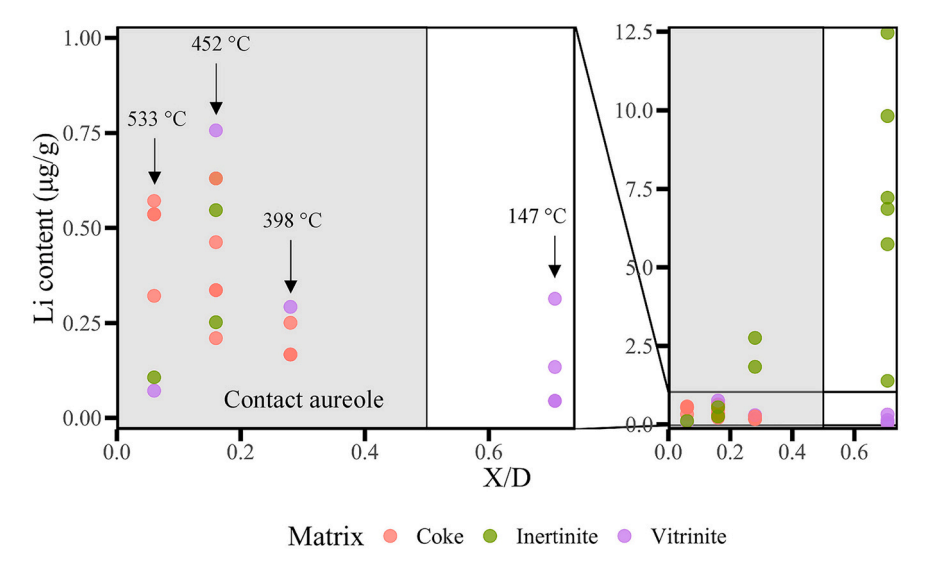


Fig. 8. Plot of Li-content measurements corrected for mass loss against X/D for Dutch Creek coal samples. Point colors indicate maceral type or coke. The plot on the left is expanded to show the lower Li-contents  $<1~\mu g/g$ . The UM sample (DC-K) has several spot measurements in inertinite grains with significantly higher Li-contents than spots measured in other samples, likely due to the silicate pore filling in the inertinite macerals.

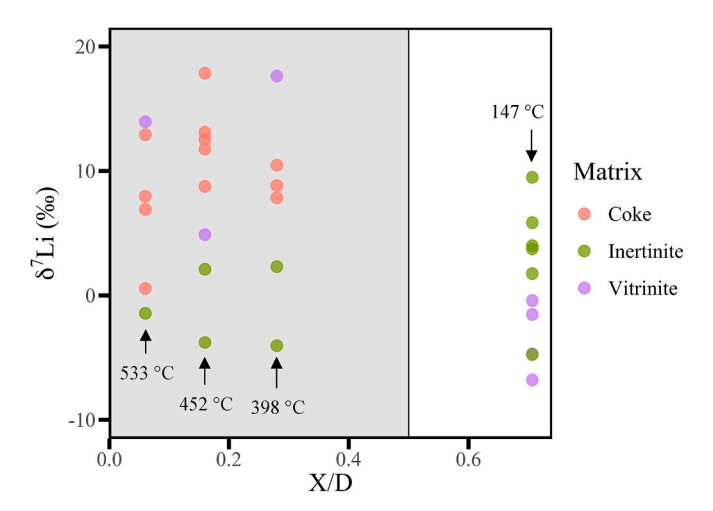


Fig. 10. Plot of  $\delta^7$ Li measurements against X/D for Dutch Creek coal samples. All samples have mean  $\delta^7$ Li values within error although there is some variation among different maceral groups and coke.

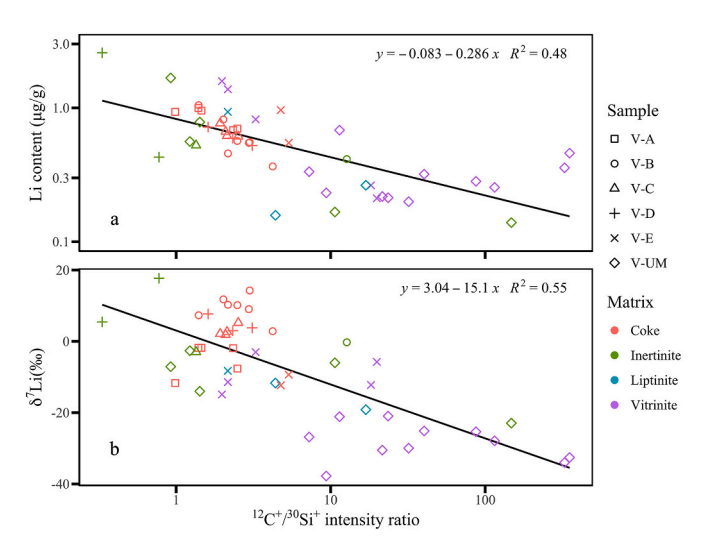


Fig. 11. Scatter plot of Vermejo coal (a) Li-contents and (b)  $\delta^7 Li$  against  $^{12}C^+/^{30}Si^+$  count ratio with the point shape indicating the sample and color indicating organic petrology. Linear regression trendlines, equations and  $R^2$  values are shown. There are weak negative correlations between both Licontent and  $^{12}C^+/^{30}Si$  ( $R^2=0.48$ ) as well as  $\delta^7 Li$  and  $^{12}C^+/^{30}Si^+$  ( $R^2=0.55$ ).

2015), while felsic porphyry intrusions are typically emplaced at temperatures ranging from 650 °C to 800 °C (Dilles et al., 2015; Meng et al., 2018; Olson et al., 2017; Schöpa et al., 2017). The higher emplacement temperature for the mafic lamprophyre dike compared to the felsic porphyry dike resulted in a wider contact aureole according to the heat flow modeling (Fig. 6). The modeled contact aureole width for the Dutch Creek coal ( $\sim$ 0.5 X/D) is consistent with the findings of Finkelman et al. (1998), who found that coal at 0.6 X/D had similar proximate, ultimate and VR<sub>o</sub> % results as samples much farther from the dike. For the Vermejo coal contact aureole the visible contact aureole was  $\sim 1$  X/D. Sample V-E, which was sampled at 0.95 X/D, had a VRo of 1.02% in comparison to 0.68% for the sample V-UM (sampled at 2.1 X/D). While no samples were collected between V-UM and V-E based on modeling results coal at just above 1 X/D also has elevated VR<sub>0</sub> % values relative to sample V-UM, more closely matching the modeled contact aureole width of 1.5 X/D.

Barker et al. (1998) found that vitrinite reflectance becomes an unreliable paleothermometer at distances within 0.3 X/D or at temperatures >300 °C and suggested this may be due to water vapor and

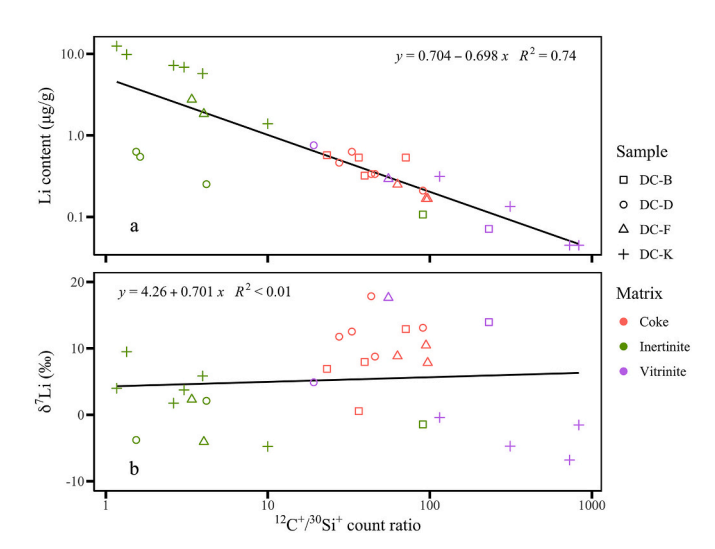


Fig. 12. Scatter plot of Dutch Creek coal (a) Li-contents and (b)  $\delta^7 \text{Li}$  against  $^{12}\text{C}^+/^{30}\text{Si}^+$  count ratio with the point shape indicating the sample and color indicating maceral type or coke. Linear regression trendlines, equations and  $R^2$  values are shown. There is negative correlation ( $R^2=0.74$ ) between the Licontent and  $^{12}\text{C}^+/^{30}\text{Si}^+$  and no correlation between  $\delta^7 \text{Li}$  and  $^{12}\text{C}^+/^{30}\text{Si}^-$ .

supercritical fluids changing the chemical evolution paths of vitrinite. Here, predicted  $T_{max}$  values derived from vitrinite reflectance (Bostick and Pawlewicz, 1984) approach the  $T_{max}$  heat-flow modeling results for the Dutch Creek coal samples (Fig. 6c), but greater deviations are observed for the higher temperature Vermejo coal samples (Fig. 6a).

#### 4.2. Contact metamorphic variations of Li-contents and Li-isotopes in coal

To evaluate chemical changes observed in the contact metamorphic zone within a single coal seam, the assumption is made that the depositional unit was relatively homogenous prior to contact metamorphism. For the Dutch Creek coal Finkelman et al. (1998) found that sample DC-K (unmetamorphosed coal) yielded similar results for proximate and ultimate analyses to samples collected much farther from the dike, thus representing the coal seam average composition. Additionally, bulk Licontents were similar in the two samples collected beyond the contact aureole (4.7 and 4.8  $\mu$ g/g) (Finkelman et al., 1998).

#### 4.2.1. Vermejo coal contact metamorphism

Coal devolatilization, refractory element concentration, and removal or addition of elements by fluids are mechanisms by which the inorganic elemental composition of a sample may change (Finkelman et al., 1998; Section 3.2, this paper). Because there are several potential mechanisms involved in changing the Li-content of coal during contact metamorphism, examining the Li-isotope composition relative to Li-contents can be useful to determine whether Li-flux occurred. However, the mean Li-contents of Vermejo coal macerals are all  $\leq$ 1.5 µg/g (Table 5) and show insignificant changes in Li-content in the contact aureole. Yet, the δ<sup>7</sup>Li values of unmetamorphosed coal (V-UM) vitrinite are 18 to 37‰ lighter than macerals within the contact aureole (Table 5; Fig. 9), suggesting there was preferential loss of <sup>6</sup>Li from macerals during contact metamorphism. Vitrinite is the most isotopically light Li maceral type in the unmetamorphosed coal with a mean  $\delta^7$ Li value of  $-28.4\% \pm 1.6$  (n= 11), which is lighter than the mean values for liptinite (-15.4%  $\pm$ 3.7; n = 2) and inertinite (-10.5%  $\pm$  3.6; n = 5) (Table 5). Any of these macerals could be a source of isotopically light Li to pore fluids and might release the Li at different thermal maturities. However, it is likely that vitrinite is the most significant here, considering that it is the most abundant organic maceral (67.2% dmmf), liptinite is minor (3.6% dmmf) and inertinite has a low potential for any hydrocarbon release (Zhou et al., 2021), which is thought to be associated with release of Li

#### from kerogen (Teichert et al., 2020; Williams et al., 2015).

According to measurements from acid leachates of low-rank coals, up to 50% of the Li may be associated with the organics (Finkelman et al., 2018). Similarly, sequential extraction of Li from Marcellus shale source rocks showed that up to 20% of the total Li may be hosted by the organic matter (Phan et al., 2016). For Li-isotopes, Li and Liu (2020) measured an organic rich Hawaiian soil and showed that the organic fraction of the soil had  $\delta^7$ Li values ~20% lighter than the mineral fractions of the soil (i.e., silicates, oxides and carbonates). The preferential accumulation of <sup>6</sup>Li in soil organic matter may be the mechanism that leads to lighter  $\delta^7$ Li values of low-rank coals compared to mature coals that appear to have preferentially released <sup>6</sup>Li (Fig. 1; Teichert et al., 2020). While the unmetamorphosed coal (V-UM) is not low-rank based on its VRo (0.68%), it is a high volatile bituminous coal that has yet to release much of its original volatile matter and hydrocarbons (Table 1). Sample V-UM is also comprised of 67.2% vitrinite (Table 2) which contains the isotopically light (-28%) Li. The weak negative correlation between  $\delta^7$ Li values and  ${}^{12}C^+/{}^{30}Si^+$  (Fig. 11b) and the 18 to 37% lighter  $\delta^7$ Li in the unmetamorphosed coal(V-UM) vitrinite compared to coke and vitrinite macerals within the contact aureole, shows that the original OM is enriched in <sup>6</sup>Li, and the metamorphism preferentially released the <sup>6</sup>Li. As isotopically light Li is released from the OM it can accumulate in pore fluids where it may eventually be incorporated into authigenic minerals. Additionally, the isotopically light Li in porefluids could become incorporated into marine carbonates which can undergo recrystallization during diagenesis (Dellinger et al., 2020), complicating paleoclimate interpretations drawn from the  $\delta^7$ Li of those carbonates. Despite the Li-contents in the unmetamorphosed Vermejo coal macerals being typically <1.5  $\mu$ g/g, porefluids could become concentrated up to ~10 μg/g with isotopically light Li from OM considering a typical coal porosity of 10% (Gan et al., 1972) leading to a rock: porefluid mass ratio in coal of  $\sim$ 12.

Because lithium is an incompatible element, it will remain in magma becoming increasingly concentrated as the magma composition evolves (Best, 2002). The mafic Morley Dike is a lamprophyre which contains phenocrysts of micas which are a likely host of Li (Woolley et al., 1996). The Li-contents of mafic magmas are  $\sim 10 \,\mu\text{g/g}$  on average and have  $\delta^7 \text{Li}$ values typically ranging from -4 to +8% (Ryan and Langmuir, 1987; Tomascak et al., 2016). Of course, as igneous intrusions ascend through country rock the Li-content of the magma and magmatic fluids can be enhanced by the assimilation of Li-rich country rock (e.g., Li-rich clays; evaporites). The Morley Dike traveled through ~1500 m of primarily Mesozoic and Paleozoic sandstone, shale, limestone, and conglomerate (Johnson and Finn, 2001) prior to reaching the Vermejo formation. If the dike was enriched in Li either from primary magma or by assimilation, it might enrich pore fluids in Li, but this is not observed in the samples studied that all show low Li-concentrations ( $\sim 1 \mu g/g$ ) in the coke and coal within the contact aureole (Fig. 7).

#### 4.2.2. Dutch Creek coal contact metamorphism

The Dutch Creek felsic porphyry intrusion, being from a more evolved magma than the mafic intrusion, was selected for comparison as it might contain higher Li-contents. At the Dutch Creek locality, macerals in sample DC-K (unmetamorphosed coal) have mean  $\delta^7$ Li values of ranging from -3.3% (vitrinite) to +3.3% (inertinite) which is consistent with the general trend for U.S. coals (Teichert et al., 2020) showing  $\delta^7$ Li as a function of VR<sub>0</sub>% (1.15%; Fig. 1). In this case, isotopically light Li may have been mostly released during burial leaving residual coal enriched in  $^7$ Li prior to dike emplacement. Vitrinite in the unmetamorphosed coal (DC-K) is isotopically lighter ( $-3.3\% \pm 0.1$ , n=4) than coke ( $+10.0\% \pm 2.5$ , n=12) and vitrinite ( $+12.2\% \pm 7.6$ , n=3) measured in the contact aureole samples, which suggests that some isotopically light organically bound Li was released upon dike emplacement.

The measured Li-contents vary widely in the unmetamorphosed coal sample (DC-K), and inertinite spot analyses with higher Li-contents

 $(1.4-12.5 \mu g/g)$  are correlated with lower  $^{12}C^+/^{30}Si^+$  (Fig. 12a) while vitrinite spots had an average Li-content of only 0.2 µg/g and higher  $^{12}\text{C}^+/^{30}\text{Si}^{\bar{+}}$  values. It is likely that during inertinite spot analyses the primary ion beam overlapped on Li-bearing clay minerals (e.g., illite, kaolinite) (Table 2) known to fill the pores of the inertinite maceral fusinite (Dai et al., 2012). Given that inertinite is oxidized organic material and has little potential for further chemical reactivity (Killops and Killops, 2004), it is an unlikely host of significant Li. Similar Li-rich spots were not measured in the samples within the contact aureole, which is likely because diagenetic silicates are in low abundance due to metamorphic recrystallization (Table 2; Finkelman et al., 1998). Notably, the bulk Li-contents (reported by Finkelman et al., 1998) are ~10 times higher for the metamorphic samples than Li-content values determined here by SIMS (Table 5). The discrepancy is likely because silicate phases containing Li were intentionally avoided in our SIMS analyses that focused on macerals, however silicate phases were included in the bulk analyses. Bulk Li-contents (Table 5; Finkelman et al., 1998) show a small increase in Li in the contact aureole of 2–3 µg/g suggesting that metamorphic silicates might have taken up Li from magmatic and/or hydrothermal fluids. Our SIMS measurements show no increase in the Licontent of the macerals measured (Table 5). If during contact metamorphism there was an overall addition of Li from dike-related fluids, the precipitation of authigenic silicate phases would take up Li from dike-related fluids, while organic-Li was being released from the

#### 4.2.3. Similarities between both contact metamorphosed coals

At both the Vermejo and Dutch Creek sampling localities vitrinite macerals in the un-metamorphosed coal samples were isotopically lighter than inertinite and liptinite macerals (Figs. 9 and 10). Inertinite and liptinite macerals tended to be more intimately associated with silicates, which may have led to overlap of the analytical crater on silicate phases, supported by the trends of  $\delta^7$ Li with  $^{12}\text{C}^+/^{30}\text{Si}$  (Figs. 11 & 12). Among all samples from the two metamorphosed coal seams, the negative correlation observed between Li-content and <sup>12</sup>C<sup>+</sup>/<sup>30</sup>Si<sup>+</sup> (Figs. 11a, 12a) suggests that Li is primarily concentrated in silicates. The question is then, what is the primary source of Li? Finkelman et al. (2018) found that on average, concentrated hydrofluoric acid leached 80% of the total Li from high rank coals and 60% of the Li from low-rank coals, which contain fewer authigenic silicates. They interpreted these results to indicate that the Li in leachates was derived solely from the silicate material. However, other studies have shown that HF digests soil OM by removing O-alkyl functional groups (Dai and Johnson, 1999) and by causing general carbon loss from OM (Rumpel et al., 2006; Rumpel et al., 2002; Schmidt et al., 1997; Zegouagh et al., 2004). In kerogen, hydrolysis, addition, and condensation reactions can occur with several organic functional groups during HF treatments (Saxby, 1976). Therefore, some organo-lithium compounds are likely digested by or react with acids such as HF and HCl (Williams and Bose, 2018).

Through electron microprobe studies of low-rank coals, Li et al. (2010; 2007) found that several inorganic elements are concentrated in vitrinite (up to 0.5% Al, 1.5% Ca, 0.1% Mg, 0.7% Fe, 0.2% Ti) that are not associated with sub-micron clay minerals based on the low Si abundances of (0.01 to 0.11%). It is probable that Li is organically bound in immature vitrinite macerals, given that Li readily substitutes for Mg, for example. Thus, the trends between Li-content and  $^{12}{\rm C}^+/^{30}{\rm Si}^+$  observed (Figs. 11a and 12a) may not be solely related to Li in silicates but also may include Li and Si associated with organic compounds, especially in low-rank coals.

# 5. Conclusions

Thermal alteration of macerals (vitrinite, liptinite, inertinite) in coal by contact metamorphism was studied to evaluate changes in the Licontent and Li-isotopic composition with temperature. One high volatile bituminous coal seam (Vermejo Fm.) was transected by a mafic dike

and another medium volatile bituminous coal seam was transected by a felsic dike (Dutch Creek Mine No.2). In addition to  $\delta^7 {\rm Li}$  changes as a function of temperature across the contact aureole, Li-contents of bulk analyses show a slight increase in Li near the Dutch Creek dike which is not observed by in situ measurements of macerals by SIMS. This may reflect uptake of Li from the felsic dike fluids by silicates in the metamorphosed coals, that was not observed in the mafic dike metamorphosed coals.

An increase in the  $\delta^7 Li$  values was observed in the high volatile bituminous Vermejo coal with proximity to the dike as temperatures increased (Fig. 9), which mirrors the trend observed for coals of different ranks from sedimentary basins across the USA (Fig. 1; Teichert et al., 2020). Isotopically light (<sup>6</sup>Li-enriched), organically bound Li in the unmetamorphosed coal vitrinite ( $-28.4\pm1.6\%$ ) is released into sedimentary pore fluids with increasing thermal maturity. The Dutch Creek coal had been heated by burial to  $\sim\!150~^\circ\text{C}$  (VRo =1.15%) before felsic dike emplacement and had likely released most of the organically bound Li during diagenesis, so there was a smaller range of  $\delta^7\text{Li}$  values among the macerals during metamorphism. However, SIMS spot analyses of vitrinite on the Dutch Creek unmetamorphosed coal (DC-K) had lighter  $\delta^7\text{Li}$  values than vitrinite and coke measured in the contact zone by 8 to 21‰ suggesting that the isotopically light organo-lithium was not entirely released during burial to 150 °C (Table 5).

The most important conclusion from this study is that isotopically light, organically bound Li released from immature kerogen during diagenesis should be considered in studies using Li-isotopes of buried sediments (e.g., marine carbonates) to reconstruct global weathering and paleoclimate. The Li-isotopic composition of pore fluids can be altered by release of <sup>6</sup>Li during organic maceral decomposition at temperatures of hydrocarbon generation and higher. The isotopically light Li in pore fluids may be incorporated into authigenic silicates and recrystallized carbonates as well, leading to possible misinterpretations of global weathering and climate in Earth's past.

# **Funding**

This work was funded by the National Science Foundation (EAR-1811613) and analytical work was supported by the ASU SIMS Facility funded by (EAR-1352996).

#### **Declaration of Competing Interest**

The authors declare that they have no known competing financial interests or personal relationships that could have appeared to influence the work reported in this paper.

# Acknowledgements

We thank Neely Bostick (USGS, Colorado, USA) for providing coal samples from Dutch Creek mine. Jedadiah Teichert and Ziliang Jin (ASU) are appreciated for assistance with field sampling. We would like to thank reviewers Dr. S. Dai, Dr. D.A. Spears, and two anonymous reviewers for their constructive comments, along with the Editor in Chief, (Dr. O. Pokrovsky).

#### Appendix A. Supplementary data

Supplementary data to this article can be found online at https://doi.org/10.1016/j.chemgeo.2022.120885.

#### References

- Annen, C., 2017. Factors affecting the thickness of thermal aureoles. Front. Earth Sci. 5, 82. https://doi.org/10.3389/feart.2017.00082.
- ASTM International, 2011. ASTM D2798-11a, Standard Test Method for Microscopical Determination of the Vitrinite Reflectance of Coal. ASTM International, West Conshohocken, PA. www.astm.org.

- ASTM International, 2013. ASTM D2799–13, Standard Test Method for Microscopical Determination of the Maceral Composition of Coal. ASTM International, West Conshohocken, PA. www.astm.org.
- ASTM International, 2015. ASTM D7582–15, Standard Test Methods for Proximate Analysis of the Analysis Sample of Coal and Coke by Instrumental Procedures. ASTM International, West Conshohocken, PA. www.astm.org.
- ASTM International, 2018a. ASTM D2013/D2013M-18, Standard Practice for Preparing Coal Samples for Analysis. ASTM International, West Conshohocken, PA. www.astm. org.
- ASTM International, 2018b. ASTM D4239-18e1, Standard Test Method for Sulfur in the Analysis Sample of Coal and Coke Using High-Temperature Tube Furnace Combustion. ASTM International, West Conshohocken, PA. www.astm.org.
- Barker, C.E., Pawlewicz, M.J., 1994. Calculation of vitrinite reflectance from thermal histories and peak temperatures. In: Vitrinite Reflectance as a Maturity Parameter, ACS Symposium Series. American Chemical Society, pp. 216–229. https://doi.org/ 10.1021/bk-1994-0570.ch014.
- Barker, C.E., Bone, Y., Lewan, M.D., 1998. Fluid inclusion and vitrinite-reflectance geothermometry compared to heat-flow models of maximum paleotemperature next to dikes, western onshore Gippsland Basin, Australia. Int. J. Coal Geol. 37, 73–111. https://doi.org/10.1016/S0166-5162(98)00018-4.
- Berner, R.A., Lasaga, A.C., Garrels, R.M., 1983. The carbonate-silicate geochemical cycle and its effect on atmospheric carbon dioxide over the past 100 million years. Am. J. Sci. 283, 641–683. https://doi.org/10.2475/ajs.283.7.641.
- Best, M.G., 2002. Igneous and Metamorphic Petrology, 2nd ed. Wiley-Blackwell.
   Bluztajn, J., Rosner, M., Ball, L., 2004. 4. 2 Inorganic and Isotope Geochemistry, 4
   O Chemistry and Material Cycles, 2004. Lithium isotope compositions of silicate reference materials. In: Presented at the 14th Annual Goldschmidt Conference, Copenhagen, Denmark.
- Bostick, N.H., 1973. Time as a factor in thermal metamorphism of phytoclasts (coaly particles). Congr. Int. Stratigr. Geol. Carbonifere Compt. Rend. 7 (1973), 183–193.
- Bostick, N.H., Collins, B.A., 1987. ABSTRACT: Petrography and Programmed Pyrolysis of Coal and Natural Coke Intruded by an Igneous Dike, Coal Basin, Pitkin County, Colorado. Presented at the The Society of Organic Petrology 4th Annual Meeting, American Association of Petroleum Geologists, p. 1.
- Bostick, N.H., Pawlewicz, M.J., 1984. Paleotemperatures based on vitrinite reflectance of shales and limestone in igneous dike aureoles in the upper cretaceous Pierre Shale, Walsenburg, Colorado. In: Hydrocarbon Source Rocks of the Greater Rocky Mountain Region. Rocky Mountain Association of Geologists, Denver, CO, p. 557.
- Chan, L.H., Edmond, J.M., 1988. Variation of lithium isotope composition in the marine environment: a preliminary report. Geochim. Cosmochim. Acta 52, 1711–1717. https://doi.org/10.1016/0016-7037(88)90239-6.
- Collins, A.G., 1975. Geochemistry of Oilfield Waters, Developments in Petroleum Science. Elsevier Scientific Pub. Co, Amsterdam; New York.
- Coombs, D.S., 1961. Some recent work on the lower grades of metamorphism. Aust. J. Sci. 24, 203–215.
- Cooper, J.R., Crelling, J.C., Rimmer, S.M., Whittington, A.G., 2007. Coal metamorphism by igneous intrusion in the Raton Basin, CO and NM: Implications for generation of volatiles. Int. J. Coal Geol. 71, 15–27. https://doi.org/10.1016/j.coal.2006.05.007.
- Dai, K.H., Johnson, C.E., 1999. Applicability of solid-state 13C CP/MAS NMR analysis in Spodosols: chemical removal of magnetic materials. Geoderma 93, 289–310. https://doi.org/10.1016/S0016-7061(99)00072-5.
- Dai, S., Jiang, Y., Ward, C.R., Gu, L., Seredin, V.V., Liu, H., Zhou, D., Wang, X., Sun, Y., Zou, J., Ren, D., 2012. Mineralogical and geochemical compositions of the coal in the Guanbanwusu Mine, Inner Mongolia, China: further evidence for the existence of an Al (Ga and REE) ore deposit in the Jungar Coalfield. Int. J. Coal Geol. 98, 10–40. https://doi.org/10.1016/j.coal.2012.03.003.
- Dai, S., Finkelman, R.B., French, D., Hower, J.C., Graham, I.T., Zhao, F., 2021. Modes of occurrence of elements in coal: a critical evaluation. Earth Sci. Rev. 222, 103815 https://doi.org/10.1016/j.earscirev.2021.103815.
- Dellinger, M., Hardisty, D.S., Planavsky, N.J., Gill, B.C., Kalderon-Asael, B., Asael, D., Croissant, T., Swart, P.K., West, A.J., 2020. The effects of diagenesis on lithium isotope ratios of shallow marine carbonates. Am. J. Sci. 320, 150–184. https://doi. org/10.2475/02.2020.03.
- Dilles, J.H., Kent, A.J.R., Wooden, J.L., Tosdal, R.M., Koleszar, A., Lee, R.G., Farmer, L.P., 2015. Zircon compositional evidence for sulfur-degassing from ore-forming arc magmas. Econ. Geol. 110, 241–251. https://doi.org/10.2113/econgeo.110.1.241.
- Eccles, D.R., Berhane, H., 2011. Geological Introduction to Lithium-Rich Formation Water with Emphasis on the Fox Creek Area of West-Central Alberta (NTS 83F and 83K) (Open File Report). Energy Resources Conservation Board, Alberta, Canada. https://ags.aer.ca/document/OFR/OFR\_2011\_10.pdf.
- Filby, R.H., van Berkel, G.J., 1987. Geochemistry of metal complexes in petroleum, source rocks and coals: An overview. In: Filby, R.H., Branthaver, J.F. (Eds.), Metal Complexes in Fossil Fuels: Geochemistry, Characterization, and Processing. American Chemical Society, Washington, D.C., pp. 2–39
- Finkelman, R.B., Bostick, N.H., Dulong, F.T., Senftle, F.E., Thorpe, A.N., 1998. Influence of an igneous intrusion on the inorganic geochemistry of a bituminous coal from Pitkin County, Colorado. Int. J. Coal Geol. 36, 223–241. https://doi.org/10.1016/ S01665162(98)00005-6.
- Finkelman, R.B., Palmer, C.A., Wang, P., 2018. Quantification of the modes of occurrence of 42 elements in coal. Int. J. Coal Geol. 185, 138–160. https://doi.org/10.1016/j. coal.2017.09.005.
- Flesch, G.D., Anderson, A.R., Svec, H.J., 1973. A secondary isotopic standard for 6Li/7Li determinations. Int. J. Mass Spectrom. 12, 265–272. https://doi.org/10.1016/0020-7381(73)80043-9.

Z. Teichert et al. Chemical Geology 602 (2022) 120885

- Galushkin, Yu.I., 1997. Thermal effects of igneous intrusions on maturity of organic matter: a possible mechanism of intrusion. Org. Geochem. 26, 645–658. https://doi. org/10.1016/S0146-6380(97)00030-2.
- Gan, H., Nandi, S.P., Walker, P.L., 1972. Nature of the porosity in American coals. Fuel 51, 272–277. https://doi.org/10.1016/0016-2361(72)90003-8.
- Hathorne, E., James, R., 2006. Temporal record of lithium in seawater: a tracer for silicate weathering? EPSL 246, 393–406. https://doi.org/10.1016/j.
- Hervig, R.L., Mazdab, F.K., Williams, P., Guan, Y., Huss, G.R., Leshin, L.A., 2006. Useful ion yields for Cameca IMS 3f and 6f SIMS: Limits on quantitative analysis. Chem. Geol. 227, 83–99. https://doi.org/10.1016/j.chemgeo.2005.09.008.
- Hettinger, R.D., Roberts, L.N.R., Gognat, T.A., 2000. Investigations of the Distribution and Resources of Coal in the Southern Part of the Piceance Basin, Colorado. US Geol. Surv. Prof. Pap., Geologic Assessment of Coal in the Colorado Plateau, Arizona, New Mexico. and Utah 1625-8\*.
- Iyer, K., Svensen, H., Schmid, D.W., 2018. SILLi 1.0: a 1-D numerical tool quantifying the thermal effects of sill intrusions. Geosci. Model Dev. 11, 43–60. https://doi.org/ 10.5194/gmd-11-43-2018.
- Jaeger, J.C., 1957. The temperature in the neighborhood of a cooling intrusive sheet. Am. J. Sci. 255 (4), 306–318. https://doi.org/10.2475/ajs.255.4.306.
- Jaeger, J.C., 1959. Temperatures outside a cooling intrusive sheet. Am. J. Sci. 257 (1), 44–54. https://doi.org/10.2475/ajs.257.1.44.
- Johnson, R.B., 1969. Geologic Map of the Trinidad Quadrangle, south-Central Colorado. Miscellaneous Geologic Investigations Map I-558.
- Johnson, R., Finn, T., 2001. Potential for a Basin-Centered Gas Accumulation in the Raton Basin, Colorado and New Mexico. US Geol. Surv. Bull., Geologic Studies of Basin Centered Gas Systems. https://doi.org/10.3133/b2184B.
- Kennedy, M.J., Wagner, T., 2011. Clay mineral continental amplifier for marine carbon sequestration in a greenhouse ocean. PNAS 108, 9776–9781. https://doi.org/ 10.1073/pnas.1018670108.
- Ketris, M.P., Yudovich, Y.A.E., 2009. Estimations of Clarkes for Carbonaceous biolithes: World averages for trace element contents in black shales and coals. Int. J. Coal Geol. 78, 135–148. https://doi.org/10.1016/j.coal.2009.01.002.
- Killops, S., Killops, V., 2004. Introduction to Organic Geochemistry. John Wiley & Sons, Ltd. https://doi.org/10.1002/9781118697214.ch4.
- Kump, L.R., Brantley, S.L., Arthur, M.A., 2000. Chemical weathering, atmospheric CO2, and climate. Annu. Rev. Earth Planet. Sci. 28, 611–667. https://doi.org/10.1146/annurey.earth.28.1.611.
- Lechler, M., Pogge von Strandmann, P.A.E., Jenkyns, H.C., Prosser, G., Parente, M., 2015. Lithium-isotope evidence for enhanced silicate weathering during OAE 1a (early Aptian Selli event). EPSL 432, 210–222. https://doi.org/10.1016/j. epsl.2015.09.052.
- Li, Wenshuai, Liu, Xiao-Ming, 2020. Lithium isotope behavior in Hawaiian regoliths: Soil-atmosphere-biosphere exchanges. Geochim. Cosmochim. Acta 285, 175–192.
- https://doi.org/10.1016/j.gca.2020.07.012.

  Li, Z., Ward, C.R., Gurba, L.W., 2010. Occurrence of non-mineral inorganic elements in macerals of low-rank coals. Int. J. Coal Geol. 81, 242–250. https://doi.org/10.1016/j.coal.2009.02.004. ICCP-TSOP 2008 Selected papers from the ICCP-TSOP joint meeting 2008: International conference on coal and organic petrology.
- Lovering, T.S., 1935. Theory of heat conduction applied to geological problems. Geol. Soc. Am. Bull. 46 (1), 69–94. https://doi.org/10.1130/GSAB-46-69.
- Macpherson, G.L., Capo, R.C., Stewart, B.W., Phan, T.T., Schroeder, K., Hammack, R.W., 2014. Temperature-dependent Li isotope ratios in Appalachian Plateau and Gulf Coast Sedimentary Basin saline water. Geofluids 14, 419–429. https://doi.org/ 10.1111/gfl.12084.
- Matjie, R.H., Li, Z., Ward, C.R., Bunt, J.R., Strydom, C.A., 2016. Determination of mineral matter and elemental composition of individual macerals in coals from Highveld mines. South. Afr. Inst. Min. Metall. 116, 169–180. https://doi.org/ 10.17159/2411- 9717/2016/v116n2a8.
- Meng, X., Mao, J., Zhang, C., Zhang, D., Liu, H., 2018. Melt recharge, f O2-T conditions, and metal fertility of felsic magmas: zircon trace element chemistry of Cu-Au porphyries in the Sanjiang orogenic belt, Southwest China. Mineral. Deposita 53, 649–663. https://doi.org/10.1007/s00126-017-0768-y.
- Millot, R., Guerrot, C., Innocent, C., Négrel, Ph., Sanjuan, B., 2011. Chemical, multiisotopic (Li-B-Sr-U-H-O) and thermal characterization of Triassic formation waters from the Paris Basin. Chem. Geol. 283, 226–241. https://doi.org/10.1016/j. chemgeo.2011.01.020.
- Misra, S., Froelich, P.N., 2012. Lithium isotope history of cenozoic seawater: changes in silicate weathering and reverse weathering. Science 335, 818–823. https://doi.org/ 10.1126/science.1214697
- Newcombe, M.E., Plank, T., Zhang, Y., Holycross, M., Barth, A., Lloyd, A.S., Ferguson, D., Houghton, B.F., Hauri, E., 2020. Magma pressure-temperature-time paths during mafic explosive eruptions. Front. Earth Sci. 8, 378. https://doi.org/10.3389/ feart 2020.531011
- Olson, N.H., Dilles, J.H., Kent, A.J.R., Lang, J.R., 2017. Geochemistry of the cretaceous Kaskanak Batholith and genesis of the Pebble porphyry Cu-Au-Mo deposit, Southwest Alaska. Am. Mineral. 102, 1597–1621. https://doi.org/10.2138/am-2017.6053
- Parr, S.W., 1922. The classification of coal. J. Ind. Eng. Chem. 14 (10), 919–922.
   Parr, S.W., 1928. The Classification of Coal, 180. University of Illinois Engineering Experiment Station Bulletin (62 p).
- Penniston-Dorland, S., Liu, X.-M., Rudnick, R.L., 2017. Lithium isotope geochemistry. Rev. Mineral. Geochem. 82, 165–217. https://doi.org/10.2138/rmg.2017.82.6.
- Phan, T.T., Capo, R.C., Stewart, B.W., Macpherson, G.L., Rowan, E.L., Hammack, R.W., 2016. Factors controlling Li concentration and isotopic composition in formation

- waters and host rocks of Marcellus Shale, Appalachian Basin. Chem. Geol. 420, 162–179. https://doi.org/10.1016/j.chemgeo.2015.11.003.
- Pogge von Strandmann, P.A.E., Jenkyns, H.C., Woodfine, R.G., 2013. Lithium isotope evidence for enhanced weathering during Oceanic Anoxic Event 2. Nat. Geosci. 6, 668–672. https://doi.org/10.1038/ngeo1875.
- Pogge von Strandmann, P.A.E., Desrochers, A., Murphy, M.J., Finlay, A.J., Selby, D., Lenton, T.M., 2017. Global climate stabilisation by chemical weathering during the Hirnantian glaciation. Geochem. Persp. Let. 230–237 https://doi.org/10.7185/ geochemlet.1726.
- Pogge von Strandmann, P.A.E.P., Kasemann, S.A., Wimpenny, J.B., 2020. Lithium and lithium isotopes in Earth's surface cycles. Elements 16, 253–258. https://doi.org/ 10.2138/gselements.16.4.253.
- Qin, S., Zhao, C., Li, Y., Zhang, Y., 2015. Review of coal as a promising source of lithium. Int. J. Oil Gas Coal T. 9, 215. https://doi.org/10.1504/IJOGCT.2015.067490.
- Rumpel, C., Kögel-Knabner, I., Bruhn, F., 2002. Vertical distribution, age, and chemical composition of organic carbon in two forest soils of different pedogenesis. Org. Geochem. 33, 1131–1142. https://doi.org/10.1016/S0146-6380(02)00088-8.
- Rumpel, C., Rabia, N., Derenne, S., Quenea, K., Eusterhues, K., Kögel-Knabner, I., Mariotti, A., 2006. Alteration of soil organic matter following treatment with hydrofluoric acid (HF). Org. Geochem. 37, 1437–1451. https://doi.org/10.1016/j. orggeochem.2006.07.001.
- Ryan, J.G., Langmuir, C.H., 1987. The systematics of lithium abundances in young volcanic rocks. Geochim. Cosmochim. Acta 51, 1727–1741. https://doi.org/ 10.1016/0016- 7037(87)90351-6.
- Saxby, J.D., 1976. Chapter 6 Chemical separation and characterization of Kerogen from Oil Shale. In: Developments in Petroleum Science. Elsevier, pp. 103–128. https://doi.org/10.1016/S0376-7361(08)70046-3.
- Schmidt, M.W.I., Knicker, H., Hatcher, P.G., Kogel-Knabner, I., 1997. Improvement of 13C and 15N CPMAS NMR spectra of bulk soils, particle size fractions and organic material by treatment with 10% hydrofluoric acid. Eur. J. Soil Sci. 48, 319–328. https://doi.org/10.1111/j.1365-2389.1997.tb00552.x.
- Schöpa, A., Annen, C., Dilles, J.H., Sparks, R.S.J., Blundy, J.D., 2017. Magma emplacement rates and porphyry copper deposits: thermal modeling of the Yerington Batholith, Nevada. Econ. Geol. 112, 1653–1672. https://doi.org/ 10.5382/econgeo.2017.4525.
- Sigmund, P., 1969. Theory of sputtering. I. Sputtering yield of amorphous and polycrystalline targets. Phys. Rev. 187 https://doi.org/10.1103/PhysRev.187.768, 769, 769
- Swaine, D.J., 1990. Mode of occurrence of trace elements in coal. In: Trace Elements in Coal. Elsevier, pp. 27–49. https://doi.org/10.1016/B978-0-408-03309-1.50008-3.
- Sweeney, J.J., Burnham, A.K., 1990. Evaluation of a simple model of vitrinite reflectance based on Chemical Kinetics (1). Am. Assoc. Pet. Geol. Bull. 74 https://doi.org/ 10.1306/0C9R251F-1710-11D7-8645000102C1865D
- Teichert, Z., Bose, M., Williams, L.B., 2020. Lithium isotope compositions of U.S. coals and source rocks: potential tracer of hydrocarbons. Chem. Geol. 549, 119694 https://doi.org/10.1016/j.chemgeo.2020.119694.
- Teichert, Z., Bose, M., Williams, P., Hervig, R.L., Williams, L.B., 2022. Secondary ion mass spectrometry reference materials for lithium in carbonaceous matrices. Geostand. Geoanal. Res. https://doi.org/10.1111/ggr.12415.
- Tomascak, P.B., Hemming, N.G., Hemming, S.R., 2003. The lithium isotopic composition of waters of the Mono Basin, California. Geochim. Cosmochim. Acta 67, 601–611. https://doi.org/10.1016/S0016-7037(02)01132-8.
- Tomascak, P.B., Magna, T., Dohmen, R., 2016. Advances in Lithium Isotope Geochemistry, Advances in Isotope Geochemistry. Springer International Publishing, Cham. https://doi.org/10.1007/978-3-319-01430-2.
- Ullmann, C.V., Campbell, H.J., Frei, R., Hesselbo, S.P., Pogge von Strandmann, P.A.E., Korte, C., 2013. Partial diagenetic overprint of late Jurassic belemnites from New Zealand: Implications for the preservation potential of δ7Li values in calcite fossils. Geochim. Cosmochim. Acta 120, 80–96. https://doi.org/10.1016/j.gca.2013.06.029.
- Wang, D., Manga, M., 2015. Organic matter maturation in the contact aureole of an igneous sill as a tracer of hydrothermal convection: a tracer of hydrothermal convection. J. Geophys. Res. Solid Earth 120, 4102–4112. https://doi.org/10.1002/ 2015.JB011877.
- Ward, C.R., 1974. Isolation of mineral matter from Australian bituminous coals using hydrogen peroxide. Fuel 53, 220–221. https://doi.org/10.1016/0016-2361(74) 90015-5.
- Williams, P., 1985. Secondary ion mass spectrometry. Annu. Rev. Mater. Sci. 34.
  Williams, L.B., Bose, M., 2018. Measurements of the lithium isotope heterogeneity in coals and kerogen indicate an unrecognized lithium contribution to the global geochemical cycles. In: CMS 55th Annual Conference, Abstract, Urbana, IL., June 2018 (2018).
- Williams, L.B., Clauer, N., Hervig, R.L., 2012. Chapter 4: Light stable isotope microanalysis of clays in sedimentary rocks. In: Quantitative Mineralogy and Microanalysis of Sediments and Sedimentary Rocks, Mineralogical Association of Canada Short Course, p. 20.
- Williams, L.B., Środoń, J., Huff, W.D., Clauer, N., Hervig, R.L., 2013. Light element distributions (N, B, Li) in Baltic Basin bentonites record organic sources. Geochim. Cosmochim. Acta 120, 582–599. https://doi.org/10.1016/j.gca.2013.07.004.
- Williams, L.B., Crawford Elliott, W., Hervig, R.L., 2015. Tracing hydrocarbons in gas shale using lithium and boron isotopes: Denver Basin USA, Wattenberg Gas Field. Chem. Geol. 417, 404–413. https://doi.org/10.1016/j.chemgeo.2015.10.027.
- Witherow, R.A., Lyons, W.B., Henderson, G.M., 2010. Lithium isotopic composition of the McMurdo Dry Valleys aquatic systems. Chem. Geol. 275, 139–147. https://doi. org/10.1016/j.chemgeo.2010.04.017.

- Woolley, A.R., Bergman, S.C., Edgar, A.D., Le Bas, M.J., Mitchell, R.H., Rock, N.M.S., Scott Smith, B.H., 1996. Classification of lamprophyres, lamproites, kimberlites, and the kalsilite, mellitic and leucitic rocks. Can. Mineral. 34, 175–186.
- You, Chen-Feng, Chan, Lui-Heung, 1996. Precise determination of lithium isotopic composition in low concentration natural samples. Geochim. Cosmochim. Acta 60 (5), 909–915. https://doi.org/10.1016/0016-7037(96)00003-8.
- Zegouagh, Y., Derenne, S., Dignac, M.F., Baruiso, E., Mariotti, A., Largeau, C., 2004. Demineralisation of a crop soil by mild hydrofluoric acid treatment: Influence on
- organic matter composition and pyrolysis. J. Anal. Appl. Pyrol. 71, 119–135. https://doi.org/10.1016/S0165- 2370(03)00059-7.
- Zhou, H., Wu, C., Pan, J., Wang, Z., Niu, Q., Du, M., 2021. Research on molecular structure characteristics of vitrinite and inertinite from bituminous coal with FTIR, Micro- Raman, and XRD spectroscopy. Energy Fuel 35 (2), 1322–1335. https://doi. org/10.1021/acs.energyfuels.0c03586.